Molecular Therapy
Original Article

LAG-3xPD-L1 bispecific antibody potentiates antitumor responses of T cells through dendritic cell activation

Eunsil Sung,[1,6] Minkyung Ko,[2,6] Ju-young Won,[3] Yunju Jo,[2,4] Eunyoung Park,[1] Hyunjoo Kim,[1] Eunji Choi,[3] Ui-jung Jung,[1] Jaehyoung Jeon,[1] Youngkwang Kim,[1] Hyejin Ahn,[3] Da-som Choi,[3] Seunghyun Choi,[2] Youngeun Hong,[1] Hyeyoung Park,[1] Hanbyul Lee,[1] Yong-Gyu Son,[1] Kyeongsu Park,[1] Jonghwa Won,[1] Soo Jin Oh,[3] Seonmin Lee,[5] Kyu-pyo Kim,[5] Changhoon Yoo,[5] Hyun Kyu Song,[4] Hyung-seung Jin,[3] Jaeho Jung,[1] and Yoon Park[2,7]

[1]ABL Bio Inc., Seongnam 13488, South Korea; [2]Theragnosis Center, Biomedical Research Institute, Korea Institute of Science and Technology (KIST), Seoul 02792, South Korea; [3]Department of Convergence Medicine, Asan Institute for Life Sciences, Asan Medical Center, University of Ulsan College of Medicine, Seoul 05505, South Korea; [4]Department of Life Sciences, Korea University, Seoul 02481, South Korea; [5]Department of Oncology, Asan Medical Center, University of Ulsan College of Medicine, Seoul 05505, South Korea

Several preclinical studies demonstrate that antitumor efficacy of programmed cell death-1 (PD-1)/programmed death-ligand 1 (PD-L1) blockade can be improved by combination with other checkpoint inhibitors. Lymphocyte-activation gene 3 (LAG-3) is an inhibitory checkpoint receptor involved in T cell exhaustion and tumor immune escape. Here, we describe ABL501, a bispecific antibody targeting LAG-3 and PD-L1 in modulating immune cell responses against tumors. ABL501 that efficiently inhibits both LAG-3 and PD-L1 pathways enhances the activation of effector $CD4^+$ and $CD8^+$ T cells with a higher degree than a combination of single anti-LAG-3 and anti-PD-L1. The augmented effector T cell responses by ABL501 resulted in mitigating regulatory-T-cell-mediated immunosuppression. Mechanistically, the simultaneous binding of ABL501 to LAG-3 and PD-L1 promotes dendritic cell (DC) activation and tumor cell conjugation with T cells that subsequently mounts effective $CD8^+$ T cell responses. ABL501 demonstrates its potent *in vivo* antitumor efficacy in a humanized xenograft model and with knockin mice expressing human orthologs. The immune profiling analysis of peripheral blood reveals an increased abundance of LAG-3^{hi}PD-1^{hi} memory $CD4^+$ T cell subset in relapsed cholangiocarcinoma patients after gemcitabine plus cisplatin therapy, which are more responsive to ABL501. This study supports the clinical evaluation of ABL501 as a novel cancer immunotherapeutic, and a first-in-human trial has started (NCT05101109).

INTRODUCTION

Somatic mutations in cancers can potentially generate neoantigens that are recognized and targeted by cytotoxic T cells.[1] However, cancer cells evolve in various ways to evade adaptive immune-mediated killing. For example, advanced tumor cells create an immunosuppressive tumor microenvironment (TME), and tumor-infiltrating T cells progressively become dysfunctional or exhausted in the TME. Exhausted T cells are characterized by decreased proliferative capacities, altered metabolism, impaired cytokine production, and sustained high-level expression of inhibitory receptors, such as programmed cell death-1 (PD-1), T cell immunoglobulin and mucin domain-containing protein 3 (Tim-3), T cell immunoreceptor with immunoglobulin and ITIM domains (TIGIT), and lymphocyte-activation gene 3 (LAG-3).[2–4] Therapeutic antibodies for blocking the interaction between PD-1 on tumor-infiltrating T cells and programmed death-ligand 1 (PD-L1) expressed on tumor cells have proven successful in the treatment of multiple cancer types. However, the proportions of patients and cancer types that can respond to anti-PD-1/PD-L1 therapies are still limited. This suggests that combination approaches may be required to generate efficient antitumor immunity and improve therapeutic outcomes.[5–7] LAG-3 is a type I transmembrane protein with four extracellular immunoglobulin (Ig)-like domains. It is primarily expressed on T cells, natural killer cells, and plasmacytoid dendritic cells (DCs). LAG-3 is upregulated during activation of T cells and plays critical roles in maintaining immune tolerance. LAG-3 has structural homology with CD4 and inhibits T cell activation by outcompeting CD4 for major histocompatibility complex class II (MHC class II) binding.[8–10] The studies by Maruhashi

Received 7 January 2022; accepted 3 May 2022;
https://doi.org/10.1016/j.ymthe.2022.05.003.

[6]These authors contributed equally

[7]Lead contact

Correspondence: Hyung-seung Jin, Department of Convergence Medicine, Asan Institute for Life Sciences, Asan Medical Center, University of Ulsan College of Medicine, Seoul 05505, South Korea.
E-mail: hsjin@amc.seoul.kr
Correspondence: Jaeho Jung, ABL Bio Inc., Seongnam 13488, South Korea.
E-mail: jaeho.jung@ablbio.com
Correspondence: Yoon Park, Theragnosis Center, Biomedical Research Institute, Korea Institute of Science and Technology (KIST), Seoul 02792, South Korea.
E-mail: ypark@kist.re.kr

et al.[11,12] showed that LAG-3 selectively recognizes a stable complex of peptides and MHC class II (pMHC-II), but not unstable pMHC-II complexes. In addition, to date, several molecules have been reported as potential ligands of LAG-3, such as LSECtin/CLEC4G, galectin-3, α-synuclein, and fibrinogen-like protein-1.[13–16] LAG-3 engagement on the T cell surface suppresses the proliferation, activation, and homeostasis of both $CD4^+$ and $CD8^+$ T cells. However, there are little data on the mechanism by which LAG-3 binding to pMHC-II modulates the activation of $CD8^+$ T cells. Several regulatory T cells (T_{reg} cell) populations have been shown to express a high and constitutive level of LAG-3, suggesting that its expression on T_{reg} cells may promote immune suppression.[17,18] However, the role of LAG-3 in the suppressive function of T_{reg} cells remains unclear. Elevated LAG-3 expression on tumor-infiltrating lymphocytes (TILs) was observed in hematologic malignancies and various solid tumors.[19] It has been reported that LAG-3 expression is associated with poor clinical outcomes.[20–22] LAG-3 is frequently co-expressed with PD-1 in TILs, and this is positively associated with T cell exhaustion. Consistent with this finding, co-blockade of LAG-3 and PD-1 augmented the proliferation and activation of antigen-specific tumor-infiltrating $CD8^+$ T cells. In several mouse preclinical models, combined treatment with anti-LAG-3 and anti-PD-(L)1 monoclonal antibodies (mAbs) has shown synergistic therapeutic effects compared with blocking either one alone.[23–25] In addition, genetic deletion of LAG3 and PD-1 has led to increased antitumor immunity and decreased tumor growth.[23,26] Several antagonist antibodies to LAG-3 are currently being evaluated in clinical trials for the treatment of solid tumors. Most recently, a LAG-3-blocking mAb (relatlimab), in combination with a PD-1 blocking mAb (nivolumab) has been approved by U.S. Food and Drug Administration (FDA) for the treatment of unresectable or metastatic melanoma. Opdualag (nivolumab and relatlimab-rmbw) showed an improved median progression-free survival compared with that in the nivolumab alone group at 10.1 (95% confidence interval [CI], 6.37–15.74) versus 4.6 (95% CI, 3.38–5.62) months, respectively, suggesting that this dual-blockade strategy is an effective treatment option.[27] Along this line, there are several bispecific antibodies targeting LAG-3 and PD-(L)1, such as MGD013, FS118, and IBI323, which are currently undergoing preclinical or early clinical studies.[28–31] Those bispecific antibodies have exhibited stronger antitumor effect over the combination of anti-PD-(L)1 and anti-LAG-3 mAbs. However, the studies have not mechanistically elucidated the advantages of the bispecific approach over a combination of mAbs. Here, we describe the generation of ABL501, a human anti-LAG-3xPD-L1 bispecific antibody (BsAb) based on anti-LAG-3 human IgG4 mAb and single-chain variable fragments (scFv) of PD-L1. We show that ABL501 directly promoted the activation of effector T cells, which led to reduction of the suppressive effect by T_{reg} cells. In addition, the LAG-3 binding arm of ABL501 enabled its engagement with PD-L1 on DCs in a context-dependent manner. Through this mechanism, ABL501 may enhance antigen cross-priming by DCs, resulting in heightened activation of $CD8^+$ T cells. Furthermore, ABL501 mediated the bridging of $LAG\text{-}3^+$ T cells and $PD\text{-}L1^+$ tumor cells, thus augmenting the antitumor cytolytic activity of $CD8^+$ T cells. Together, these findings indicated that bispecific antibody ABL501 may have superior antitumor potency compared with the combination of LAG-3 and PD-L1 mAbs.

RESULTS

ABL501 enhances effector T cell responses by blocking the LAG-3 and PD-L1 pathways

ABL501, a bispecific antibody targeting human LAG-3 and PD-L1, was constructed from an anti-LAG-3 monoclonal IgG4 antibody and a scFv for PD-L1, which is fused at the C terminus of the anti-LAG-3 antibody via a $(G4S)_3$ linker, with an amino acid substitution (S224P) in the hinge region of IgG4 to reduce the formation of half-antibodies (Figure 1A).[32] Moreover, the scFv domain is composed of light- and heavy-chain variable regions connected by a $(G4S)_4$ linker. The binding of ABL501 to either recombinant human LAG-3 or PD-L1 was measured via surface plasmon resonance (SPR) and ELISA (Figure S1). In addition, comparable binding capacity between ABL501 and anti-LAG-3 or anti-PD-L1 mAbs was observed in Jurkat cells expressing LAG-3 or SNU324 cells endogenously expressing PD-L1 (Figure 1B). As ABL501 was developed in the human IgG4 isotype, Fc-mediated effector functions, including antibody-dependent cellular cytotoxicity (ADCC) and complement-dependent cytotoxicity (CDC), were not elicited by ABL501 (Figure S2). We then assessed the ability of ABL501 to block the binding between PD-1 and PD-L1 or LAG-3 and MHC class II (Figures 1C and S3). A dual blocking effect by ABL501 was comparable to the combination of anti-LAG-3 and anti-PD-L1 single antibody treatment, as measured using bioassays in LAG-3 and PD-1 expressing nuclear factor κB (NF-κB)-Luc2 reporter Jurkat cells. Next, to examine the potency of ABL501 on human T cell activation under physiological conditions, we stimulated $CD3^+$ T cells with allogeneic monocyte-derived DCs (mo-DCs) in the presence of anti-LAG-3 and/or anti-PD-L1 or ABL501. Upregulation of both LAG-3 and PD-1 was found in activated $CD4^+$ or $CD8^+$ T cells upon stimulation with allogeneic mo-DCs that expressed human leukocyte antigen-DR isotype (HLA-DR) and PD-L1 (Figure S4). Dual blockade of LAG-3 and PD-L1 by the combination or ABL501 treatment increased the proliferative capacity of both $CD4^+$ and $CD8^+$ T cells in a similar extent (Figure 1D). However, an even greater increase in interferon (IFN)-γ secretion by both $CD4^+$ and $CD8^+$ T cells was observed following ABL501 treatment at a low concentration of 8.35 nM than the combination of anti-LAG-3 and anti-PD-L1 that showed a synergistic effect on IFN-γ compared with PD-L1 blockade alone (Figure 1E). These results indicate that co-blockade of LAG-3 and PD-L1 by ABL501 efficiently promotes the activation of both $CD4^+$ and $CD8^+$ effector T cells.

ABL501 mitigates T_{reg}-cell-mediated immunosuppression by augmenting effector T cell responses

LAG-3 has been known to be highly expressed on T_{reg} cells, but the role of LAG-3 in modulating T_{reg} cell responses remains controversial.[33] We therefore investigated whether ABL501 contributes to weaken T_{reg} cell function. Instead of using a T_{reg} mixed lymphocyte reaction assay,[34,35] we employed A375 cells expressing

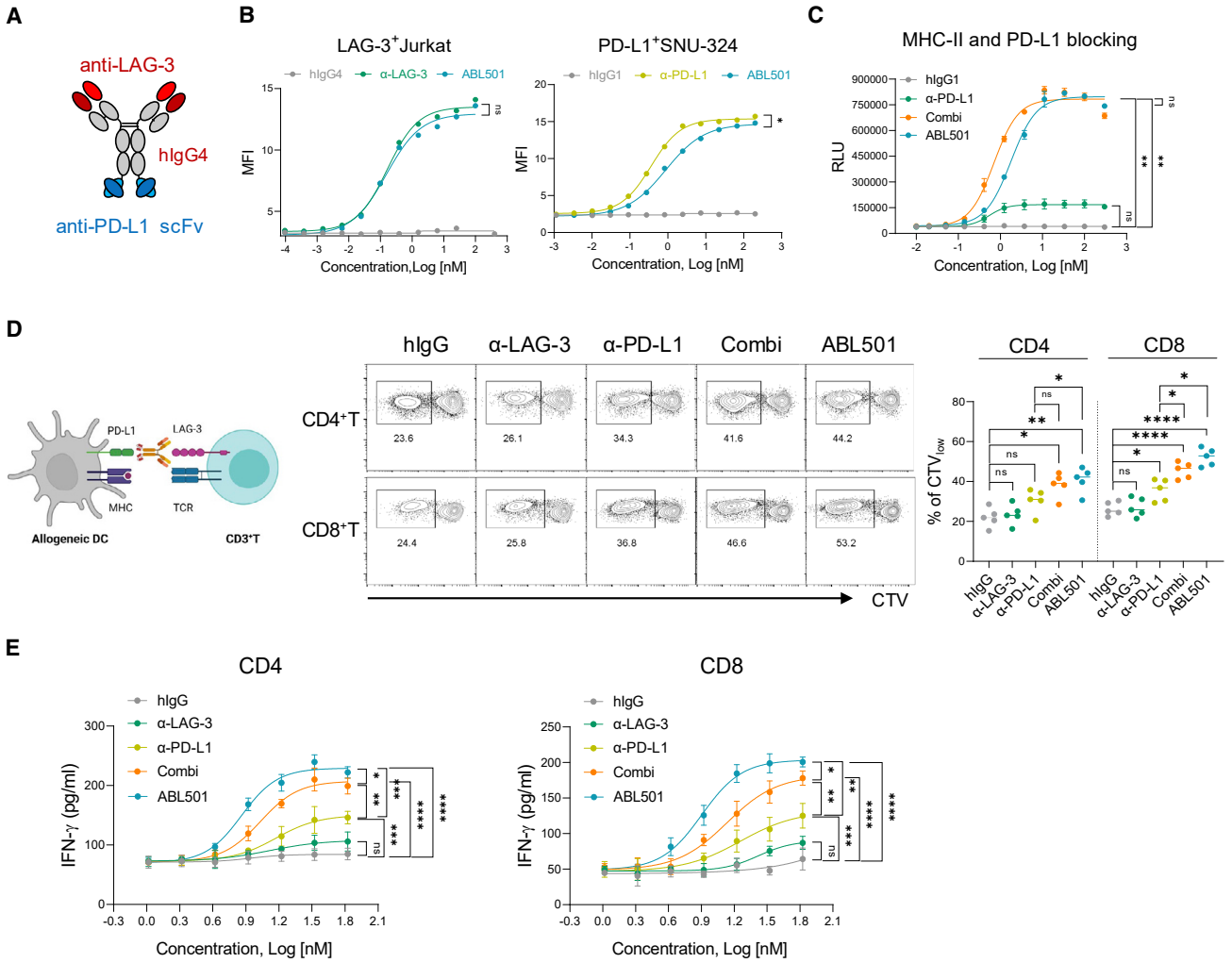

Figure 1. ABL501 augments effector T cell activation by the inhibition of both LAG-3 and PD-L1 axes

(A) Schematic of LAG-3xPD-L1 BsAb, ABL501. (B) FACS analysis of ABL501 or anti-LAG-3 binding to LAG-3 and PD-1 expressing Jurkat cells (left panel) is shown (ABL501: half-maximal effective concentration [EC_{50}] = 0.15 nM; anti-LAG-3: EC_{50} = 0.16 nM). FACS analysis of ABL501 or anti-PD-L1 binding to endogenously PD-L1 expressing SNU-324 cells (right panel) is shown (ABL501: EC_{50} = 0.87 nM; anti-PD-L1: EC_{50} = 0.36 nM). (C) LAG-3 and PD-1 expressing NF-κB-Luc2 reporter Jurkat cells were co-incubated with target cells expressing MHC-II and PD-L1 in the presence of the indicated antibodies at various concentrations. Blocking activity was analyzed by measuring luminance of the downstream NF-κB reporter (ABL501: EC_{50} = 1.78 nM, Combi: EC_{50} = 0.7 nM, and anti-PD-L1: EC_{50} = 0.53 nM). (D and E) $CD4^+$ T or $CD8^+$ T cells isolated from PBMCs were co-cultured with allogeneic mo-DCs in the presence of the indicated antibodies at various concentrations for 5 days. (D) Schematic illustration of mixed lymphocyte reaction (MLR) assay (left panel) is shown. FACS analysis shows CTV dilution of $CD4^+$ and $CD8^+$ T cells with the indicated antibodies at a final concentration of 33.4 nM. Representative FACS plots (above) and a summary plot (below) show the percentages of CTV_{low} $CD4^+$ and $CD8^+$ T cells. Each dot represents an individual human sample. (E) ELISA of IFN-γ secretion by $CD4^+$ T cells (left; ABL501: EC_{50} = 7.27 nM, Combi: EC_{50} = 10.78 nM, anti-PD-L1: EC_{50} = 14.9 nM, and anti-LAG-3: EC_{50} = 14.07 nM) or by $CD8^+$ T cells (right; ABL501: EC_{50} = 7.99 nM, Combi: EC_{50} = 13.61 nM, anti-PD-L1: EC_{50} = 18.04 nM, and anti-LAG-3: EC_{50} = 26.28 nM). Data were compiled from three to five independent experiments with two replications. Statistical significance was determined by one-way ANOVA with Holm-Sidak multiple comparisons. *$p < 0.05$, **$p < 0.01$, ***$p < 0.001$, ****$p < 0.0001$, and ns, not significant.

membrane-bound anti-CD3 scFv (A375-OKT3) as a stimulator to avoid disparities between effector T and T_{reg} cells for alloantigen recognition. $CD8^+$ or $CD25^-CD127^+CD4^+$ T cells were co-cultured with A375-OKT3 cells in the presence or absence of autologous $CD4^+CD25^+Foxp3^+$ T_{reg} cells that were fluorescence-activated cell sorting (FACS) sorted ($CD4^+CD25^+CD127^-$) and *ex vivo* expanded with interleukin-2 (IL-2) and transforming growth factor β (TGF-β) (Figures 2A and 2B). Co-culture with T_{reg} cells induced a robust suppression of both proliferative capacity and IL-2 secretion in $CD4^+$ or $CD8^+$ T cells (Figures 2C and 2D). In the presence of T_{reg} cells, the combination of anti-LAG-3 and anti-PD-L1 increased proliferation and IL-2 secretion by both effector $CD4^+$ and $CD8^+$ T cells, and ABL501 more efficiently relieved effector T cells from T_{reg}-cell-mediated suppression (Figures 2E and 2F). However, when

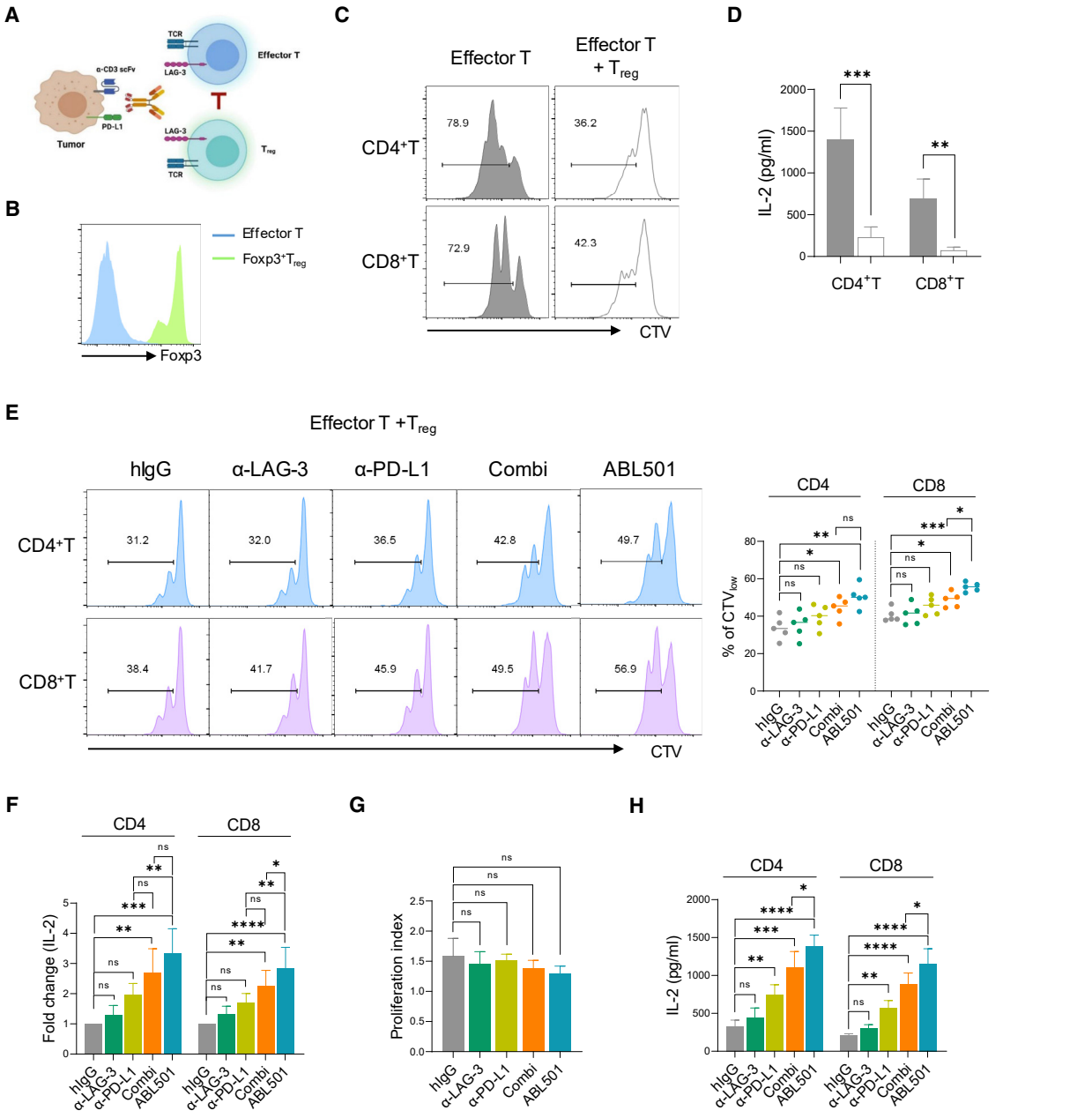

Figure 2. ABL501 weakens T_{reg}-mediated suppression through promoting effector T cell responses

(A–F) FACS sorted and *ex vivo* expanded $CD25^+CD127^-CD4^+$ T_{reg} cells were co-cultured with conventional $CD4^+$ or $CD8^+$ T cells isolated from the same human donor in the presence of A375 melanoma cells expressing membrane-bound anti-CD3 scFv (A375-OKT3). (A) Schematic illustration of the *ex vivo* human T_{reg} cell suppression assay is shown. (B) FACS analysis of Foxp3 expression in *ex vivo* expanded T_{reg} cells is shown. (C and D) FACS analysis showing CTV dilution (C) or ELISA of IL-2 secretion (D) by $CD4^+$ T or $CD8^+$ T cells in the presence or absence of T_{reg} cells (effector T: T_{reg} = 4:1) is shown. (E and F) FACS analysis shows CTV dilution (E) or ELISA of IL-2 secretion (F) by $CD4^+$ T or $CD8^+$ T cells with the indicated antibodies at a final concentration of 66.8 nM in the presence of T_{reg} cells. (G) Isolated and *ex vivo* expanded T_{reg} cells were co-cultured with A375-OKT3 cells in the presence of the indicated antibodies at a final concentration of 66.8 nM. Proliferation index of T_{reg} cells was calculated by FlowJo software based on CTV dilution. (H) Isolated conventional $CD4^+$ or $CD8^+$ T cells were co-cultured with A375-OKT3 cells in the presence of the indicated antibodies at a final concentration of 66.8 nM. ELISA of IL-2 secretion by $CD4^+$ T or $CD8^+$ T cells is shown. Data were pooled from three to five independent experiments with two replications. Statistical significance was determined by unpaired t tests with two-tailed analysis in (D) or one-way ANOVA with Holm-Sidak multiple comparisons in (E)–(H). *$p < 0.05$, **$p < 0.01$, ***$p < 0.001$, ****$p < 0.0001$, and ns.

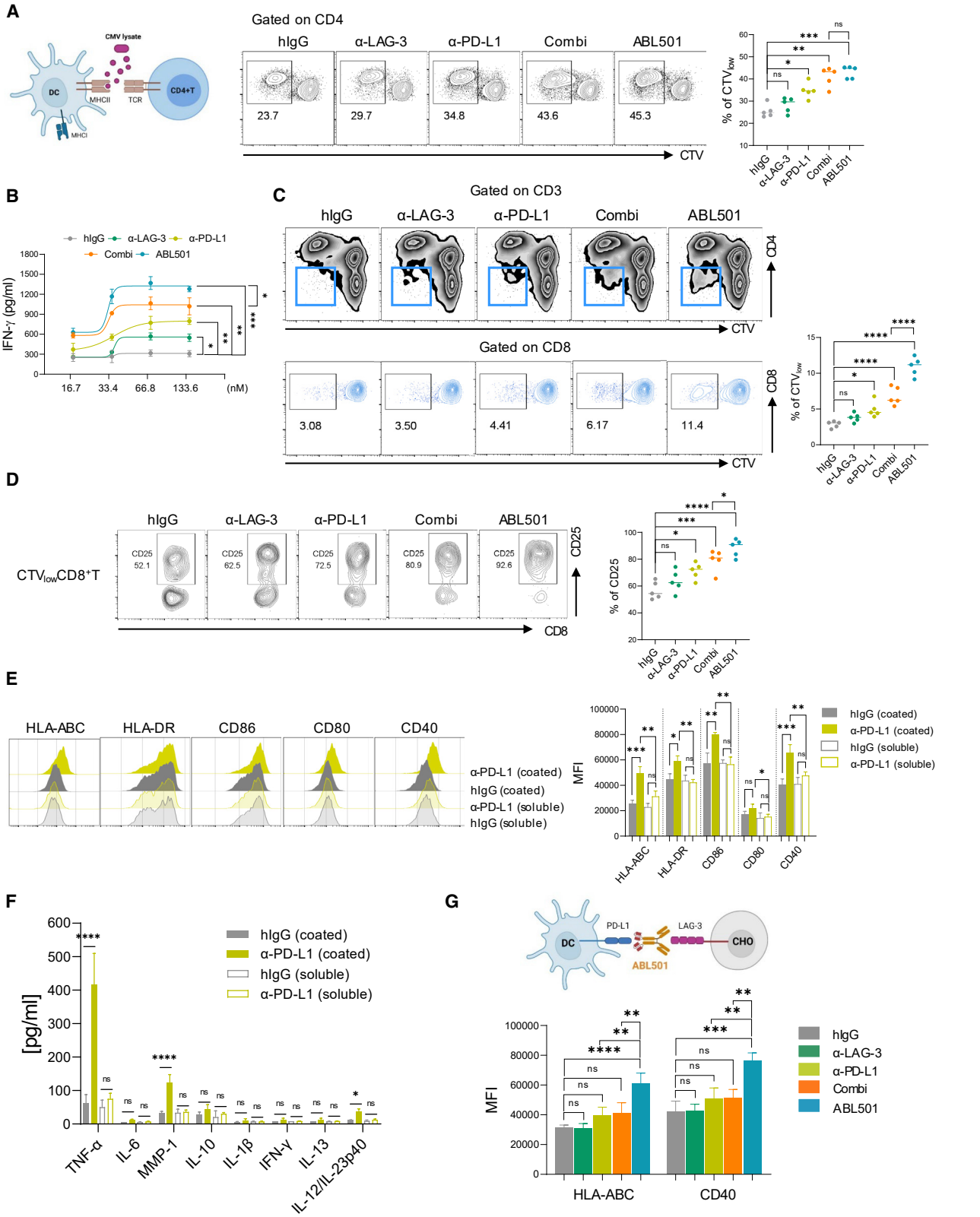

(legend on next page)

T_{reg} cells were stimulated by A375-OKT3 cells in the absence of effector T cells, single or dual blockade of LAG-3 and/or PD-L1 largely unaltered T_{reg} cell proliferation and phenotypic marker expressions that are known as key features of highly suppressive $CD45RO^+$ T_{reg} cells (Figures 2G and S5).[36] Unlike T_{reg} cells, effector T cell activation was augmented upon ABL501 treatment (Figure 2H), which suggested that co-blockade of LAG-3 and PD-L1 by ABL501 compensates the suppressive effect of T_{reg} cells by promoting effector T cell activation rather than directly affecting T_{reg} cell responses.

ABL501 induces $CD8^+$ T cell activation by promoting DC maturation

We then investigated the mechanism by which ABL501 promotes both $CD4^+$ and $CD8^+$ T cell responses. First, we assessed the effect of ABL501 on antigen-specific $CD4^+$ memory T cell responses in cytomegalovirus (CMV)-seropositive donors upon stimulation with CMV lysate that was presented by MHC class II on DCs.[37] Co-blockade of LAG-3 and PD-L1 by the combination treatment with anti-LAG-3 and anti-PD-L1 or ABL501 enhanced CMV-specific $CD4^+$ T cell expansion compared with LAG-3 or PD-L1 blockade alone (Figure 3A). Despite the comparable expansion rate of $CD4^+$ T cells, ABL501 treatment resulted in a higher secretion of IFN-γ, IL-2, and tumor necrosis factor alpha (TNF-α) than the co-treatment with anti-LAG-3 and anti-PD-L1 (Figures 3B and S6). Although CMV lysate primarily triggers MHC-class-II-restricted $CD4^+$ T cell responses, CMV-specific $CD8^+$ T cell activation can also be induced by MHC-class-I-mediated cross-presentation of CMV antigen in DCs. Indeed, we found that co-blockade of LAG-3 and PD-L1 mounted CMV-responsive $CD8^+$ T cell populations, and this effect was more significant with ABL501 treatment (Figure 3C). ABL501 treatment not only increased the expansion rate but also the activation level, as indicated by CD25 expression frequencies in CMV-responsive $CD8^+$ T cells, compared with anti-LAG-3 and anti-PD-L1 co-treatment (Figure 3D). This suggests that the induction of CMV-responsive $CD8^+$ T cell expansion by ABL501 results in increased IFN-γ secretion upon CMV lysate stimulation, compared with the combination treatment with anti-LAG-3 and anti-PD-L1. It has been reported that reverse signaling via PD-L1 ligation with PD-1 inhibits DC maturation and activation,[38] which can be restored by PD-L1 or PD-1 blockade.[39,40] We reasoned that a strong PD-L1-blocking effect by LAG3xPD-L1 BsAb may promote DC activation. To test this hypothesis, we assessed the expression of co-stimulatory receptors, including HLA-ABC, HLA-DR, CD86, CD80, and CD40 on mo-DCs at 48 h after treatment with plate-coated or soluble anti-PD-L1. DCs incubated with plate-coated anti-PD-L1, which mimics an immobilized anti-PD-L1 by the bispecific format of ABL501, exhibited more activated phenotype with increased expression of activation markers compared with DCs treated with soluble anti-PD-L1 (Figure 3E). Furthermore, a marked increase in TNF-α, MMP-1, and IL-12 secretion was shown by DCs incubated with plate-coated anti-PD-L1, even without lipopolysaccharide (LPS) stimulation (Figure 3F). We then confirmed the strong PD-L1-blocking effect of ABL501 on DC activation by employing LAG-3-expressing Chinese hamster ovary (CHO) cells (CHO-LAG-3) as a matrix for anti-LAG-3 binding, which allowed to avoid extrinsic effects on DCs by T cell activation in response to ABL501 treatment. Both HLA-ABC and CD40 expressions were upregulated in DCs when they were co-incubated with CHO-LAG-3 cells in the presence of ABL501 (Figure 3G). Collectively, these results imply that ABL501 can promote DC maturation for antigen cross-priming and subsequent $CD8^+$ T cell activation.

ABL501 potentiates $CD8^+$ T cell cytotoxicity by promoting conjugation with tumor cells

We next investigated whether ABL501 directly affects $CD8^+$ T cell responses against tumor. To measure the cytotoxic activity of $CD8^+$ T cells against tumor cells, we employed 1G4 T cell receptor (TCR)-expressing $CD8^+$ T cells that specifically recognize NY-ESO-1 cancer testis antigen (NY-ESO-1: 157–165 epitope) expressed by cancer cells in an HLA-A*0201-restricted manner (Figure 4A).[41] Co-culture of A375 cells endogenously expressing A2-NY-ESO-1 with 1G4 TCR-$CD8^+$ T cells led to efficient killing of A375 cells in a dose-dependent manner, compared with TCR non-transduced (NT) $CD8^+$ T-cell-mediated A375 killing, which is probably caused by allogeneic responses of $CD8^+$ T cells against tumor cells (Figure S7). Treatment with ABL501 resulted in an increased killing rate of A375 cells by 1G4 TCR-$CD8^+$ T cells, compared with combination treatment with single anti-LAG-3 and anti-PD-L1 at various concentrations (Figure 4B) or at effector:target (E:T) ratio of 1:10 and 1:20 (Figure 4C). In addition, 1G4 TCR-$CD8^+$ T cells led to higher IFN-γ levels upon ABL501 treatment, compared with co-treatment with anti-LAG-3 and anti-PD-L1 (Figure 4D). Consistent with

Figure 3. ABL501 promotes DC maturation to induce $CD8^+$ T cell activation

(A–E) CTV-stained PBMCs were stimulated with CMV lysate in the presence of the indicated antibodies at various concentrations for 5 days. (A) Schematic illustration of CMV lysate assay (above) is shown. Representative FACS plots (left panel) and a summary plot (right panel) showing the percentages of proliferating $CD4^+$ T cells (CTV_{low}) with the indicated antibodies at a final concentration of 66.8 nM are shown. (B) ELISA of IFN-γ secretion by CMV-responsive T cells with the indicated antibodies at various concentrations is shown. (C) Representative FACS plots show proliferating $CD8^+$ populations (CTV_{low}) in $CD3^+$ T cells (above) or the percentages of CTV_{low} $CD8^+$ T cells (gated on $CD8^+$ T; below) with the indicated antibodies at a final concentration of 66.8 nM. (D) Representative FACS plots (left panel) and a summary plot (right panel) show the percentages of CD25 expression in CMV-specific (CTV_{low}) $CD8^+$ T cells. Data were compiled from five independent experiments with two replicates. (E and F) mo-DCs were incubated with plate-coated or soluble anti-hIgG or anti-PD-L1 for 2 days. (E) Representative FACS histograms showing the expression of HLA-ABC, HLA-DR, CD86, CD80, and CD40 in mo-DCs (left panel). Summary graph shows the geometric mean fluorescence intensity (MFI) of the expression of the indicated markers in mo-DCs (right panel). (F) Multiplex cytokine assay of the secretion of the indicated cytokines in mo-DCs is shown. (G) Schematic illustration of an *in vitro* DC activation assay (above). mo-DCs were incubated with CHO-LAG-3 cells in the presence of the indicated antibodies at a final concentration of 66.8 nM for 2 days. Summary graph shows the geometric MFI of the expression of the indicated markers in mo-DCs (below). Data were pooled from three independent experiments with two replicates. Statistical significance was determined by one-way ANOVA with Holm-Sidak multiple comparisons. *$p < 0.05$, **$p < 0.01$, ***$p < 0.001$, ****$p < 0.0001$, and ns.

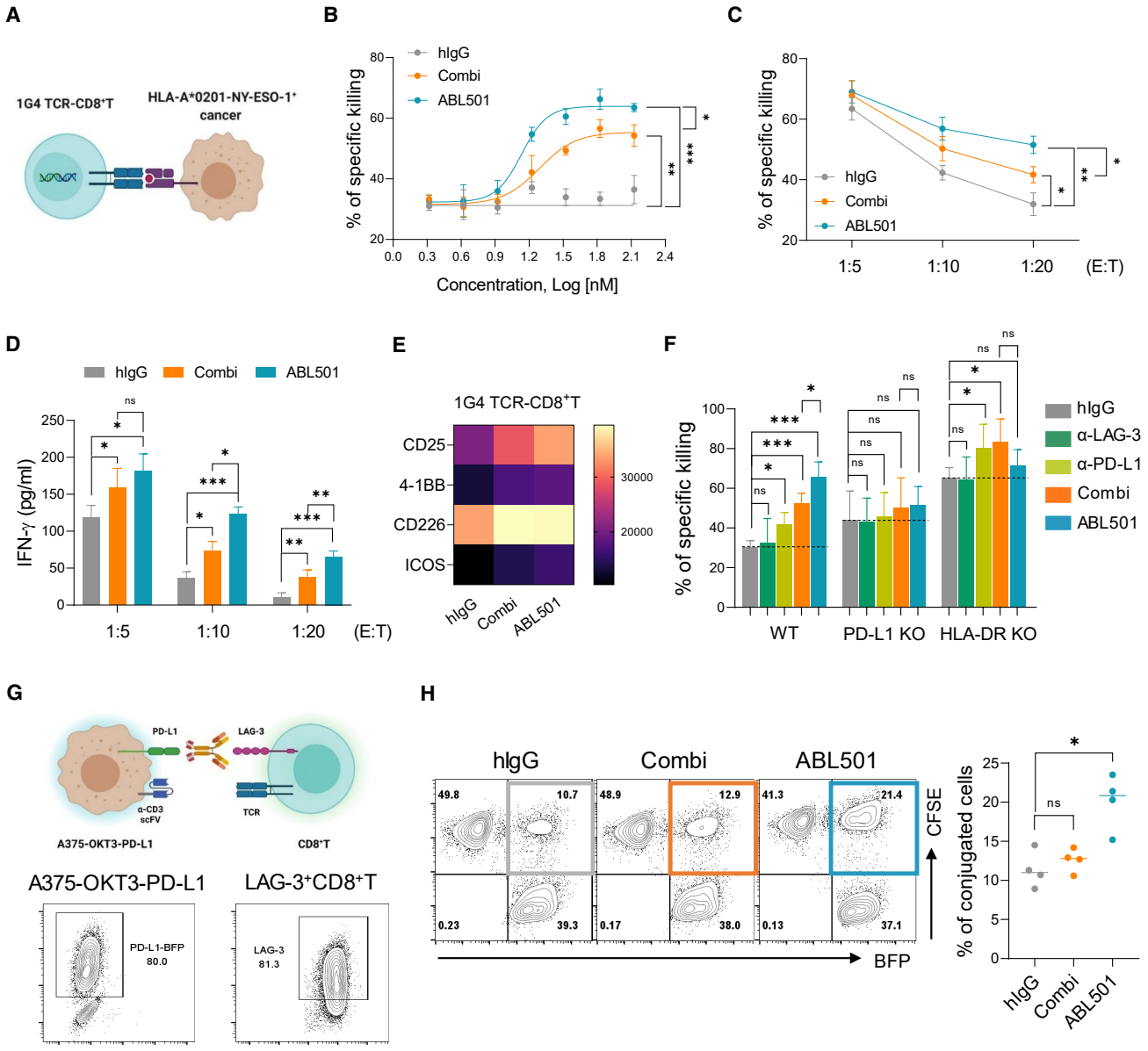

Figure 4. ABL501 plays a bridging role between CD8⁺ T cells and tumors to enhance tumor cell killing

(A–E) 1G4 TCR-engineered CD8⁺ T (1G4 TCR-CD8⁺ T) cells were co-cultured with A375 cells expressing HLA-A*0201-restricted peptide NY-ESO-1 (157-165) at variable E:T ratios for 2 days in the presence of the indicated antibodies at various concentrations. (A) Schematic illustration of 1G4 TCR-engineered CD8⁺ T-cell-mediated tumor cell killing is shown. (B) Percentages of NY-ESO-1-specific killing of A375 cells at E:T ratio of 1:10 in the presence of the indicated antibodies at various concentrations are shown. (C and D) Percentages of NY-ESO-1-specific killing of A375 cells (ABL501: EC_{50} = 13.6 nM; Combi: EC_{50} = 19.5 nM) (C) or ELISA of IFN-γ secretion by 1G4 TCR-CD8⁺ T cells (D) at the indicated E:T ratios in response to combination treatment with anti-LAG-3 and anti-PD-L1 or ABL501 at a final concentration of 66.8 nM are shown. (E) Heatmap plot shows the geometric MFI of the expression of co-stimulatory molecules by 1G4 TCR-CD8⁺ T cells at E:T ratio of 1:10 in the presence of the indicated antibodies at a final concentration of 66.8 nM. (F) Percentages of NY-ESO-1-specific killing of wild-type (WT), PD-L1-deficient (PD-L1 KO), or HLA-DR-deficient (HLA-DR KO) A375 cells by 1G4 TCR-CD8⁺ T cells at an E:T ratio of 1:10 in the presence of the indicated antibodies at a final concentration of 66.8 nM are shown. Data were pooled from three independent experiments with three replicates. (G and H) CFSE-labeled CD8⁺ T cells expressing LAG-3 by pre-activation with anti-CD3/CD28 antibodies were incubated with A375-OKT3 cells expressing PD-L1-BFP for 30 min in the presence of the indicated antibodies at a final concentration of 66.8 nM, followed by FACS analysis. (G) Schematic illustration of T-cell-tumor conjugation assay (above) is shown. Representative FACS plots show PD-L1-BFP expression by A375-OKT3 cells and LAG-3 expression by pre-activated CD8⁺ T cells (below). (H) Representative FACS plots (left panel) and a summary plot (right panel) show the percentages of BFP and CFSE double-positive populations in the presence of the indicated antibodies. Data were compiled from four independent experiments with two replicates. Statistical significance was determined by one-way ANOVA with Holm-Sidak multiple comparisons in (B)–(D), (F), and (H). *p < 0.05, **p < 0.01, ***p < 0.001, and ns.

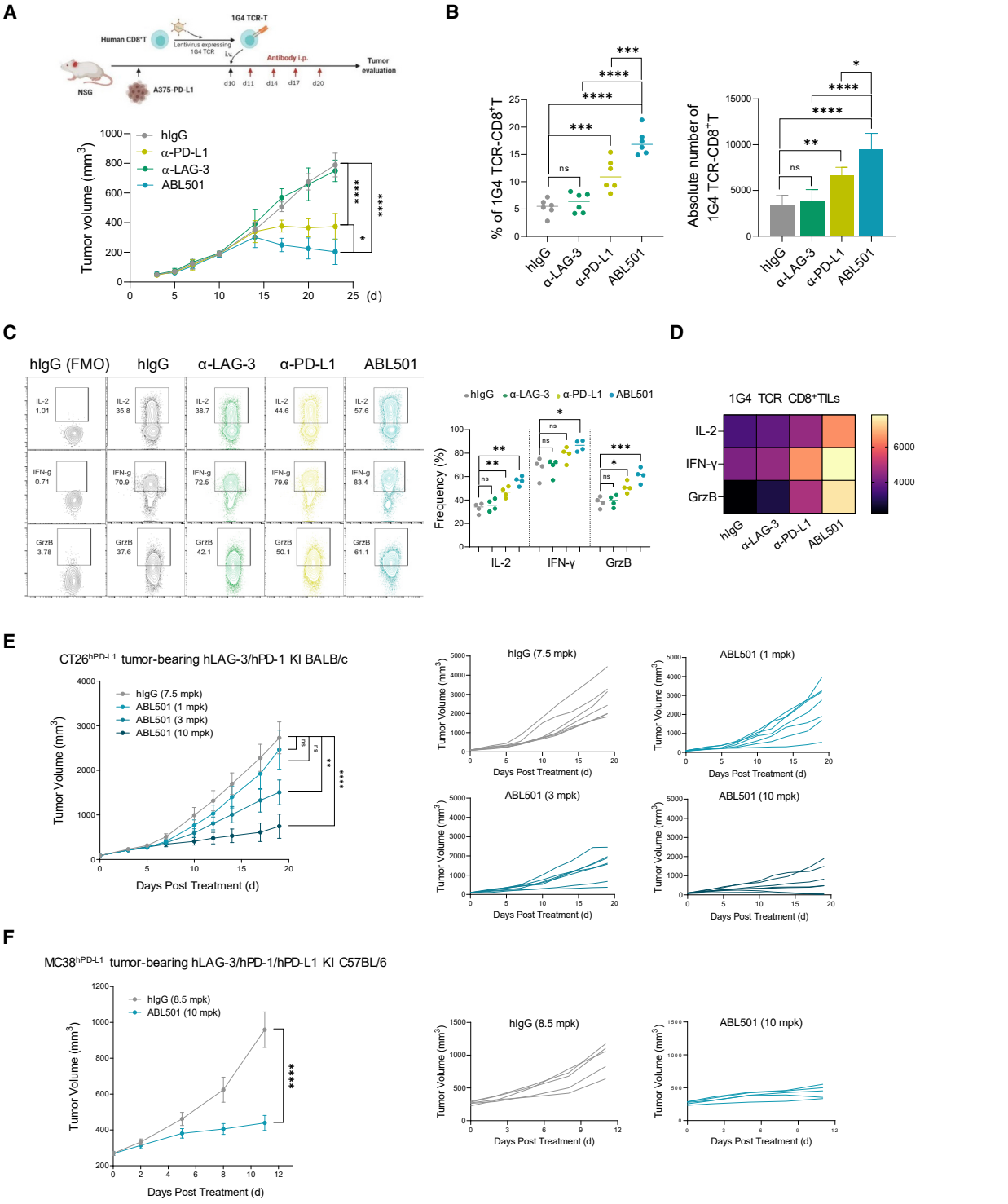

Figure 5. ABL501 treatment exerts antitumor effects in mouse tumor models

(A–D) 1G4 T cells expressing an NY-ESO-specific TCR were adoptively transferred into NSG mice bearing A375-PD-L1 tumors. At 1 day following T cell transfer, the mice were intraperitoneally treated with hIgG4 (10 mg/kg), anti-LAG3 (10 mg/kg), anti-PD-L1 (10 mg/kg), or ABL501 (14 mg/kg, molar equivalent amount) on days 11, 13, 17, and 20 (five mice/group). Tumor samples were collected on day 21 and processed for single-cell suspensions and then subjected to FACS analysis. (A) Experimental scheme of an *in vivo* xenograft mouse tumor model (above). Mice were monitored for tumor growth, and means ± SEM of n = 5 mice/group are shown (below). (B) Summary plots

(legend continued on next page)

the enhanced effector responses of 1G4 TCR-CD8$^+$ T cells by ABL501, upregulation of co-stimulatory markers, including CD25, 4-1BB, CD226, and ICOS, was observed in ABL501-treated 1G4 TCR-CD8$^+$ T cells at 48 h after co-culture with A375 cells (Figure 4E). We then wanted to evaluate whether ABL501 requires simultaneous binding with both LAG-3 and PD-L1 to enhance 1G4 TCR-CD8$^+$ T cell activation. To test this, we generated HLA-DR- or PD-L1-knockout (KO) A375 cells (Figure S8). ABL501 did not show an enhanced killing effect on HLA-DR KO or PD-L1 KO A375 cells by 1G4 TCR-CD8$^+$ T cells, whereas the combination treatment retained its PD-L1-blocking effect in HLA-DR KO A375 cells (Figure 4F), which confirm that the effect of ABL501 is dependent on simultaneous binding to LAG-3 and PD-L1. We further elaborated how ABL501 elicits a higher cytotoxic activity in 1G4 TCR-CD8$^+$ T cells against tumor cells than the combination of anti-LAG-3 and anti-PD-L1. Because bispecific T cell engagers are known to exert antitumor immune responses by assembling immunological synapse between T cells and tumor cells,[42] we hypothesized that ABL501 acts as a T cell engager by bridging between CD8$^+$ T cells and tumor cells. To test this hypothesis, we performed a conjugation assay using A375-OKT3-PD-L1 (BFP$^+$) and carboxyfluorescein diacetate succinimidyl ester (CFSE)-labeled CD8$^+$ T cells expressing LAG-3 (LAG-3$^+$CD8$^+$ T) by pre-activation with anti-CD3 and anti-CD28 (Figure 4G). When LAG-3$^+$CD8$^+$ T cells were incubated with A375-OKT3-PD-L1 cells in the presence of a combination of anti-LAG-3 and anti-PD-L1, we observed no significant increase in the BFP and CFSE double-positive population, compared with incubation with the control hIgG. In contrast, ABL501 treatment increased LAG-3$^+$CD8$^+$ or CD4$^+$ T cell conjugation with A375-OKT3-PD-L1 cells (Figures 4H and S9), suggesting that ABL501 acts as a bridge facilitating tumor cell engagement with T cells.

Antitumor efficacy of ABL501 in humanized mouse tumor models

Considering that the binding arms of ABL501 do not cross-react with murine LAG-3 and PD-L1 molecules, the efficacy of ABL501 *in vivo* was assessed in humanized mouse models. First, we utilized a humanized tumor xenograft model. This model evaluates the efficacy of therapeutics to modulate antigen-specific cytolytic activity of an infused CD8$^+$ T cell against implanted tumors expressing specific MHC-antigen complexes. We implanted A375-PD-L1 tumors into immunodeficient non-obese diabetic (NOD)-severe combined immunodeficiency (SCID) IL-2Rγ^{null} (NSG) mice and adoptively transferred 1G4 TCR-T cells (Figure 5A). In mice bearing A375-PD-L1 tumors, adoptive transfer of 1G4 TCR-T cells was able to control tumor growth, compared with the no T cell transfer group (Figure S10A). Treatment with the parental anti-LAG-3 alone did not suppress tumor growth compared with control IgG treatment. The parental anti-PD-L1 treatment exhibited approximately 50% tumor growth inhibition (TGI), but tumors continued to grow. Notably, treatment with ABL501 yielded significant tumor regression (Figure 5A, bottom). To explore the antitumor activity mechanisms of ABL501, we analyzed TILs following the final treatment with antibodies. Anti-PD-L1 treatment increased the percentage and number of transferred CD8$^+$ T cells in tumors. In contrast, anti-LAG-3 antibody had no effect on CD8$^+$ TIL persistence. The frequency and number of 1G4 TCR CD8$^+$ TILs were significantly higher in the ABL501-treated groups than in the other groups (Figure 5B). In addition, ABL501 treatment increased the frequency and expression level of IL-2, IFN-γ, and granzyme B by 1G4 TCR CD8$^+$ TILs, compared with treatment with either parental antibody (Figures 5C and 5D). These results indicate that ABL501 potentiates antigen-specific CD8$^+$ T cell responses against tumor. Next, we evaluated the *in vivo* antitumor efficacy of ABL501 using humanized transgenic BALB/c mice expressing human LAG-3 and PD-1. Human PD-L1 knockin CT26 cells (CT26^{hPD-L1}) were implanted into the transgenic mice, followed by intraperitoneal administration of test antibodies. ABL501 exerted potent antitumor activity over a broad dose range of 1, 3, and 10 mg/kg (TGI = 22.8%, 30.2%, and 71.9%, respectively), resulting in improved overall survival (Figure 5E). The antitumor effect of ABL501 (10 mg/kg) was further confirmed in human PD-L1 knockin MC38 cells (MC38^{hPD-L1}) bearing humanized transgenic C57BL/6 mice expressing human LAG-3, PD-1, and PD-L1 (Figure 5F). ABL501 treatment at all doses did not produce significant toxicity, as indicated by body weight measurements in mice (Figures S10B and S10C). We also assessed the safety of ABL501 in cynomolgus monkeys that were administered ABL501 at 0, 20, 60, or 200 mg/kg twice weekly, eight times. ABL501 was well tolerated up to 200 mg/kg/dose with a safe toxicity profile in cynomolgus monkeys (Figures S11A–S11C). In addition, treatment with ABL501 did not induce the secretion of pro-inflammatory cytokines, including IL-2, IFN-γ, IL-6, and TNF-α, by peripheral blood mononuclear cells (PBMCs) (Figure S11D).

LAG-3^{hi}PD-1^{hi} memory CD4$^+$ T cell signatures contribute to predicting the response to ABL501 in cholangiocarcinoma patients

Immune checkpoint inhibitor therapies are commonly used in the second-line setting in a variety of advanced solid malignancies after progression on standard-of-care treatment. To identify

showing the percentages (left panel) and numbers (right panel) of 1G4 TCR-CD8$^+$ T cells in tumors per treatment group. (C) Representative FACS plot (left panel) and summary plot (right panel) show the percentages of IL-2, IFN-γ, or granzyme B by 1G4 TCR-CD8$^+$ T cells in tumors per treatment group. (D) Heatmap plot shows the geometric MFI of the expression of the indicated cytokines by tumor infiltrating 1G4 TCR-CD8$^+$ T cells. (E) CT26 cells with knockin human PD-L1 were subcutaneously injected into human LAG-3/PD-1 knockin BALB/c mice (n = 6–8/group). Mice were treated with the indicated concentrations of ABL501 three times at 7-day intervals. Tumor growth curves of individual mice (right panel) are shown. (F) MC38 cells with knockin human PD-L1 were subcutaneously injected into human LAG-3/PD-1/PD-L1 knockin C57BL/6 mice (n = 5/group). Mice were treated with ABL501 (10 mg/kg) or isotype control (8.5 mg/kg) four times at 3-day intervals. Tumor growth curves of individual mice (right panel) are shown. Significant differences between groups were determined by two-way ANOVA Tukey's multiple comparison test. *$p < 0.05$, **$p < 0.005$, ***$p < 0.001$, ****$p < 0.001$, and ns.

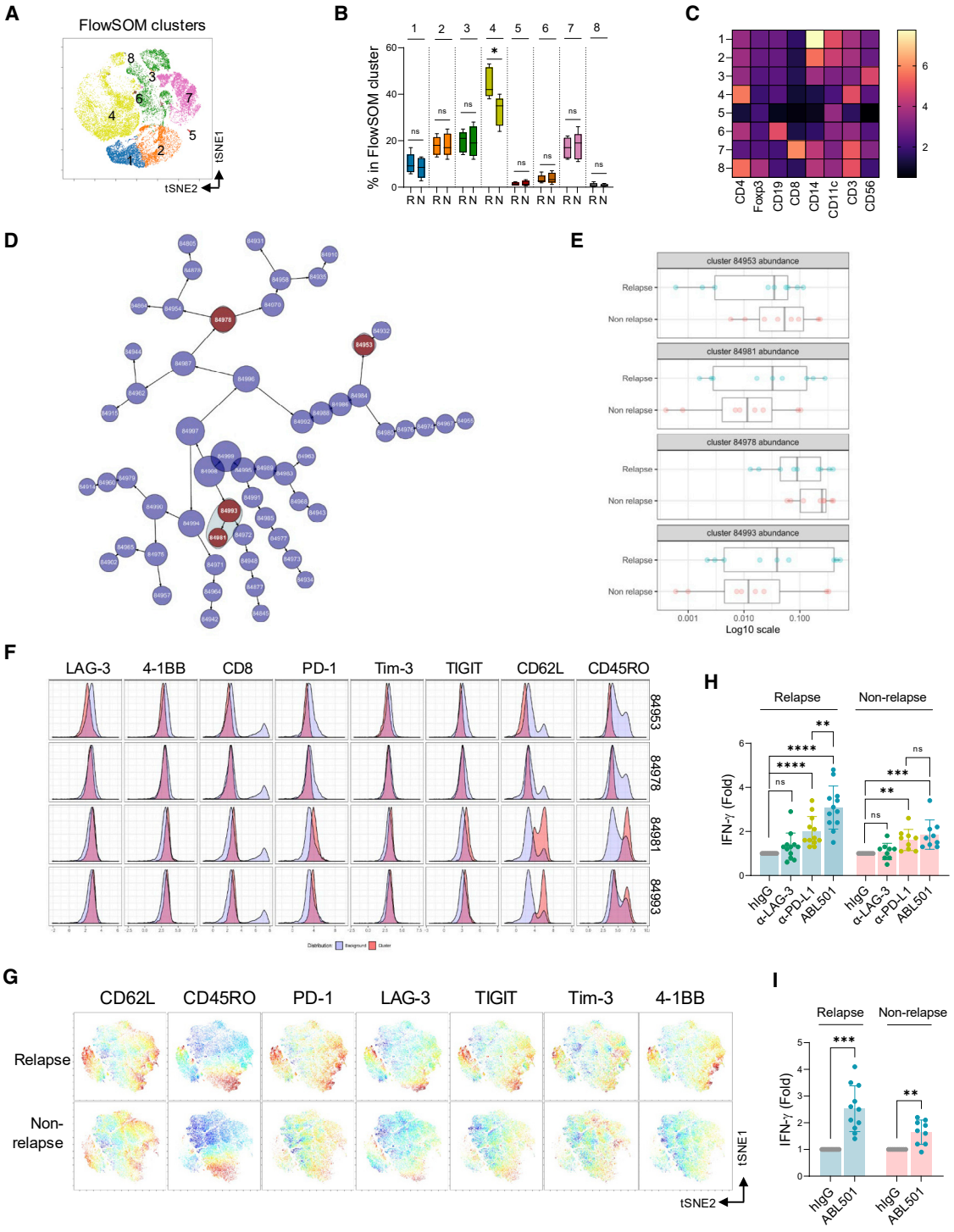

Figure 6. Abundance of LAG-3^{hi}PD-1^{hi} memory CD4^{+} T cells in peripheral blood of CCA patients was correlated with response to ABL501

(A–C) FlowSOM analysis of immune cell subsets in the peripheral blood of relapsed (n = 10) or non-relapsed (n = 9) CCA patients. (A) viSNE plot shows immune cell subset clusters to identify FlowSOM clustering. (B) Bar graph shows the frequencies of each cluster in two groups (relapse versus non-relapse). (C) Heatmap shows the MFI of each cluster. (D–F) CITRUS analysis of T cell signatures in the peripheral blood of relapsed (n = 9) or non-relapsed (n = 8) CCA patients is shown. (D) CITRUS plot shows clusters from CCA patients in two groups (relapse versus non-relapse). Red dots represent clusters that showed a different abundance with a statistical significance between groups. (E) Bar graphs show the relevance of abundance for the selected clusters (red dots) between groups. (F) Histogram plots show each marker expression by the selected

(legend continued on next page)

characteristics of peripheral blood T cells that relate to LAG-3xPD-L1 BsAb responsiveness, we next analyzed the expression of immune cell markers in the peripheral blood of cholangiocarcinoma (CCA) patients after therapy with gemcitabine plus cisplatin (GemCis), a standard regimen for advanced CCA (Figure S12).[43,44] High-dimensional flow cytometry and self-organizing map (FlowSOM) algorithm were used to cluster immune cells based on the expression of immune cell markers, including CD3, CD4, CD8, Foxp3, CD19, CD56, CD14, and CD11c, and also to compare the abundance of each metacluster between relapsed and non-relapsed patients after GemCis therapy (Figures 6A and 6B). Frequencies of cells in cluster 4, which represents non-T_{reg} $CD4^+$ T cells (Figures 6B and 6C), were increased in relapsed patients compared with those in non-relapsed patients, suggesting a role of non-T_{reg} $CD4^+$ T cells in clinical responses. The abundance of non-T_{reg} $CD4^+$ T cell populations in relapsed patients was also shown by cluster identification, characterization, and regression (CITRUS) algorithm that allows the discovery of statistically significant signatures by unsupervised hierarchical clustering (Figure S13).[45] We then further assess the phenotypic characteristics of both $CD4^+$ and $CD8^+$ T cells in CCA patients using CITRUS analysis (Figure 6D). Among four clusters (red dots) that were identified by CITRUS analysis, two (84953 and 84978) had a phenotype of $CD62L^-CD45RO^-$ effector $CD4^+$ T cells with a lower expression of LAG-3, 4-1BB, PD-1, Tim-3, and TIGIT, and the abundance of these clusters was increased in non-relapsed patients after GemCis therapy (Figures 6E and 6F). In contrast, the other two clusters (84981 and 84993) that represented $CD62L^{hi}CD45RO^{hi/int}$ memory $CD4^+$ T cells were more abundant in relapsed patients than in non-relapsed patients. $CD4^+$ T cells in these clusters presented an activated phenotype with high expression levels of LAG-3, 4-1BB, PD-1, Tim-3, and TIGIT, showing an opposite expression profile from clusters 84993 and 84978. Similarly, these phenotypic differences of $CD4^+$ T cells between relapsed and non-relapsed patients after GemCis therapy were visualized by t-distribution stochastic neighbor embedding (viSNE) analysis (Figure 6G). We next questioned which $CD4^+$ T cell signatures were more responsive to ABL501 treatment. $CD3^+$ T cells from patients were co-cultured with A375-OKT3 cells in the presence of anti-LAG-3, anti-PD-L1, or ABL501. $CD3^+$ T cells in relapsed patients who had a greater abundance of $CD62L^{hi}$ memory $CD4^+$ T cells with high expression levels of LAG-3 and PD-1 were more responsive to ABL501 treatment than $CD3^+$ T cells in non-relapsed patients (relapse: 3.08-fold; non-relapse: 1.85-fold) (Figure 6H). Similar results were observed for PBMC stimulation with a peptide pool (CEF+NY-ESO-1+MART1+) that induces antigen-specific $CD8^+$ T cell responses. ABL501 efficiently augmented IFN-γ secretion by antigen-specific $CD8^+$ T cells in relapsed patients compared with that in non-relapsed patients (relapse: 2.52-fold; non-relapse: 1.64-fold) (Figure 6I), indicating that the abundance of $LAG\text{-}3^{hi}PD\text{-}1^{hi}$ memory $CD4^+$ T cell subset has potential predictive value for ABL501 therapy.

DISCUSSION

Therapeutic strategies for restoring T cell activity via co-blocking of LAG-3 and PD-1/PD-L1 with mAbs have proven to be beneficial in preclinical tumor models[23,24] and humans.[46–48] Especially with the FDA approval of Opdualag (nivolumab and relatlimab-rmbw),[27] new approaches targeting LAG-3 and PD-(L)1 with BsAbs, which are expected to allow more selective binding of antibodies and a simultaneous blockade of both LAG-3 and PD-(L)1, have been actively developed in the preclinical and early clinical stages.[28–31] However, despite the apparent benefits of BsAb, the functional and mechanistic advantages of dual blocking of LAG-3 and PD-(L)1 by BsAb over a combination of anti-LAG-3 and anti-PD-(L)1 mAbs are still unclear.

Our study revealed that ABL501, a BsAb targeting LAG-3 and PD-L1, promoted antigen cross-presentation by DCs and subsequently induced $CD8^+$ T cell activation to a higher extent than a combination treatment with anti-LAG-3 and anti-PD-L1 mAbs. This result highlights the benefit of co-blocking LAG-3 and PD-L1 with the BsAb. As it has been shown that PD-1/PD-L1 pathway blockade enhances DC maturation and activation,[38–40] the observed effect of ABL501 in DCs might come from the anti-PD-L1 part of the BsAb, which is expected to provide either a stronger blocking effect or more stable binding to PD-L1 on DCs than anti-PD-L1 mAbs. Indeed, we observed enhanced mo-DC activation with the plate-coated anti-PD-L1, but not with the soluble anti-PD-L1 treatment.

Although PD-L1 blockade directly affected DC activation, co-blockade of LAG-3 and PD-L1 mounted a higher level of $CD8^+$ T cell responses upon CMV lysate stimulation compared with LAG-3 or PD-L1 blockade alone, which implies that LAG-3 blockade can contribute to PD-L1 blockade-mediated DC activation. One possible explanation is that LAG-3 blockade can augment CMV-specific $CD4^+$ T cell responses, accompanied by an increased secretion of IFN-γ, IL-2, and TNF-α, supporting DC activation and leading to the subsequent cross-priming of $CD8^+$ T cells.[49–51] A recent study suggested that treatment with LAG-3xPD-L1 BsAb increased soluble LAG-3 (sLAG-3) levels by promoting the shedding of LAG-3 from the cell surface, although it is unclear how LAG-3xPD-L1 BsAb induced the proteolytic cleavage of surface LAG-3.[29] Because a recombinant sLAG-3Ig protein has been reported to stimulate the maturation of DCs or macrophages by competitively binding to MHC class II against surface LAG-3,[52–55] increased sLAG-3 by

clusters (red) over background (light blue). (G) Representative viSNE plots of $CD4^+$ T cells in the peripheral blood of relapsed or non-relapsed CCA patients overlaid with the expression of naive, memory, co-inhibitory, or co-stimulatory markers. (H) Fold increase of IFN-γ secretion by $CD3^+$ T cells from relapsed (n = 12) or non-relapsed (n = 9) CCA patients upon co-culture with A375-OKT3 in the presence of the indicated antibodies at a final concentration of 66.8 nM is shown. (I) Fold increase of IFN-γ secretion by peptide pool-treated peripheral blood $CD8^+$ T cells obtained from relapsed (n = 11) or non-relapsed (n = 9) CCA patients in the presence of the indicated antibodies at a final concentration of 66.8 nM is shown. Statistical significance was determined by paired t tests with two-tailed analysis in (B) or one-way ANOVA with Holm-Sidak multiple comparisons in (H) and (I). *$p < 0.05$, **$p < 0.005$, ***$p < 0.001$, ****$p < 0.001$, and ns.

LAG-3xPD-L1 BsAb was suggested as an indicator of T cell or DC activation.[29] However, unlike recombinant sLAG-3Ig protein, the role of sLAG-3 or its binding to MHC class II is unknown,[56,57] warranting further investigation of its biological relevance.

Cross-presenting conventional DC1s (cDC1s) that efficiently mount $CD8^+$ T cell responses against exogenous antigens, such as tumor antigens, have been highlighted as a target of cancer vaccines.[58–60] Recent approaches to deliver cancer vaccines specifically into cDC1s have shown promising results in preclinical settings, with an efficient induction of antigen-specific effector or memory $CD8^+$ T cells and tumor regression.[61–63] In this regard, the novel mechanism of ABL501 in regulating cross-presenting DCs not only suggests a non-redundant benefit of our bispecific antibody approach but also provides a rationale for therapeutic strategies, including combination with cross-presenting, DC-targeting cancer vaccines.

Aside from this DC-mediated mechanism through which ABL501 promotes $CD8^+$ T cell activation, we also found that ABL501 can directly enhance the cytotoxic activity of $CD8^+$ T cells against tumor cells by promoting $CD8^+$ T cell conjugation with tumor cells. A recent study also showed a bridging function of LAG-3xPD-L1 BsAb in LAG-3- or PD-L1-overexpressing cell lines without TCR engagement,[64] but it insufficiently addressed the bridging role of LAG-3xPD-L1 BsAb in a situation where T cells are engaged with tumor cells through pMHC-I-TCR binding. We employed NY-ESO-1-specific, TCR-engineered (1G4 TCR) $CD8^+$ T cells to address the mechanistic and functional roles of ABL501 against NY-ESO-1-expressing tumor cells under a more physiological condition. ABL501 treatment resulted in nearly complete tumor regression in A375-PD-L1-bearing NSG mice subjected to adoptive transfer of 1G4 TCR-$CD8^+$ T cells, which argues that ABL501 can sufficiently support the antitumor responses of $CD8^+$ T cells without the intervention of $CD4^+$ T cells. Another advantage of this model is that it provides a unique opportunity to study the biology of human tumor antigen-specific $CD8^+$ TILs, which would allow better prediction of patients' responses to T-cell-targeting reagents, including ABL501.[65] Regardless of these obvious benefits, this model cannot fully recapitulate human tumor microenvironment due to the NSG mouse background. We exploited human LAG-3, PD-1, and PD-L1 knockin (KI) syngeneic mouse models to compensate for the limitation of the xenograft model. ABL501 showed an ability to elicit efficient antitumor responses by immune cells in the intact tumor microenvironment, which further supports its potential as cancer immunotherapeutics. However, we cannot rule out the possibility that the reconstitution of human receptors affects endogenous immune responses in KI mice. Therefore, further investigation about the modulation of TILs by ABL501 and its translational value is warranted.

Identification and characterization of the major immune cell populations responding to immune checkpoint inhibitor (ICI) therapies are crucial for their clinical success, emphasizing the importance of immune-monitoring studies in cancer patients. Compared with $CD8^+$ T cell subsets that have been intensively investigated in the context of predicting clinical responses to ICI therapies,[66,67] the characteristics and predictive value of $CD4^+$ T cell subsets, other than T_{reg} cells, are less well known, despite the importance of $CD4^+$ T cell support for the antitumor immune responses of $CD8^+$ T cells.[68] Recent studies have reported the correlation between $CD4^+$ T cell immunity and clinical responses to PD-1/PD-L1 blockade in cancer patients.[69–71] In particular, one study used the immune monitoring of peripheral blood from patients with non-small cell lung cancer to show that the frequency of $CD62L^{lo}$ $CD4^+$ T cells is a predictive biomarker.[70]

Our immune-monitoring studies also revealed that the decreased abundance of $CD62L^{lo}CD45RO^{lo}$ effector $CD4^+$ T cell populations in peripheral blood was correlated to disease recurrence in patients with CCA after GemCis therapy. Conversely, LAG-3^{hi}PD-$1^{hi}CD62L^{hi}$ memory $CD4^+$ T cells exhibiting an activated phenotype with high expression of both co-stimulatory and inhibitory markers were more abundant in relapsed CCA patients, which implicates the slower kinetics of GemCis-therapy-induced $CD4^+$ T cell activation or repopulation. A correlation between the LAG-3^+ immunotype in peripheral blood and poor clinical outcomes was also found in patients with melanoma or urothelial carcinoma after anti-PD-1 or anti-CTLA-4 therapies.[64] This $CD4^+$ T cell phenotype in relapsed CCA patients turned out to be beneficial for eliciting T cell responses upon ABL501 treatment. In relapsed patients, ABL501-mediated T cell activation might involve not only the $CD62L^+$ memory characteristics but also the increased LAG-3 expression on $CD4^+$ T cells. Although the expression level of immune checkpoint receptors on T cells is not always positively correlated with the clinical response rate, as shown in PD-1 expression and anti-PD-1 blockade,[72] it was reported in a small cohort study that melanoma patients with higher LAG-3 expression on TILs were more responsive to a combination of relatlimab (BMS-986016) plus nivolumab.[46] Our study therefore proposes new treatment strategies for LAG-3xPD-L1 BsAb therapy in combination with chemotherapies and offers novel criteria for patient stratification.

In summary, our study illustrates the divergent ability of LAG-3xPD-L1 bispecific antibody to enhance the potency of T cell activation and highlights how this bispecific antibody can exert the immune modulation not achievable by a combination of mAbs. The favorable toxicity profile and potent antitumor activity of ABL501 support its clinical evaluation in patients with cancer.

MATERIALS AND METHODS

Cell lines

A375, Jurkat, and HCC1954 cells were purchased from American Type Culture Collection (CRL-1619, TIB-152, and CRL-2338). SNU-324 cells were obtained from Korean Cell Line Bank (KCLB) (00324). CHO-S cells were purchased from Invitrogen. All cells were maintained as recommended by the suppliers.

Stable cell line generation

A375 cell lines stably expressing firefly luciferase and/or human PD-L1 were generated (A375-Fluc, A375-PD-L1, and A375-Fluc-PD-L1)

using a Sleeping Beauty transposon system.[73] Full-length human PD-L1 gene was cloned into a bicistronic BFP expression vector, pSBbi-BP (Addgene plasmid no. 60512). For the generation of T cell stimulator cells, A375-Fluc and A375-Fluc-PD-L1 cells were infected with a lentivirus encoding mouse anti-human CD3 (OKT3) scFv fused to CD28 transmembrane domain (A375-Fluc-OKT3 and A375-Fluc-PD-L1-OKT3). OKT3 scFv expression on cell surface was verified by FACS using an anti-mouse IgG antibody. PD-L1 or HLA-DR in A375-Fluc cells was knocked out via CRISPR-Cas9. The guide sequences (PD-L1: 5′-TCTTACCACTCA GGACTTGA-3′, HLA-DR: 5′-GAGTACTGGAACAGCCAGA-3′, designed by the CRIPSPR Gold online tool) were cloned into pX330-mCherry vector (Addgene plasmid no. 98750). A375-Fluc cells were transfected with single guide RNA (sgRNA)-expressing plasmids, and the resulting transfected cells were single cell subcloned.[74]

Mixed lymphocyte reaction (MLR) assay

Human $CD3^+$ T cells were separated form PBMCs using an EasySep Human T cell Isolation Kit (STEMCELL Technologies). $CD3^+$ T cells were stained with CellTrace Violet (CTV) (Invitrogen). The proliferation of T cells was evaluated by measuring CTV dilution by flow cytometry. To assess allospecific T cell activation, $CD14^+$ monocytes were separated from allo-PBMCs using MojoSort Human CD14 Nanobeads (BioLegend) and cultured in complete RPMI 1640 medium with granulocyte-macrophage colony-stimulating factor (GM-CSF) (80 ng/mL) and IL-4 (80 ng/mL) for 5 days. Allogenic immature DCs were co-cultured with CTV-stained $CD3^+$ T cells for 5 days at a ratio of 15:1 (T:DC).

1G4 TCR-T cell assay

A lentiviral vector encoding a 1G4 TCR that recognizes the HLA-A*0201 restricted NY-ESO-1 peptide (NY-ESO-1:157-165) was generated in the pHR lentiviral backbone (Addgene plasmid no. 79125). Lentivirus was generated by transient transfection of 293FT cells with the packaging plasmids psPAX2 (Addgene plasmid no. 12260) and pVSVg (Addgene plasmid no. 8454). Human primary $CD8^+$ T cells were isolated from PBMCs and stimulated with Dynabeads Human T-Activator CD3/CD28 (Invitrogen) in the presence of IL-2 (100 ng/mL; Peprotech). A lentivirus encoding a 1G4 TCR was transduced into $CD8^+$ T cells 3 days after the stimulation by spinoculation in the presence of polybrene (8 μg/mL). The expression of 1G4 TCR was assessed by flow cytometric analysis using an anti-human Vβ13.1 TCR chain antibody (BioLegend).

CMV lysate assay

To analyze recall responses of memory T cells in an antigen-specific manner, PBMCs were treated with 100 ng/mL of CMV lysates (Microbix Biosystems) for 5 days. T cell responses were evaluated by IFN-γ ELISA and CTV dilution assays.

Human T_{reg} cell suppression assay

$CD3^+CD4^+CD25^+CD127^-$ T_{reg} cells were isolated from PBMCs and stimulated with Dynabeads Human T-Activator CD3/CD28 (Invitrogen) at a cell-to-bead ratio of 4:1 in complete RPMI 1640 medium with IL-2 (100 ng/mL; Peprotech) and TGF-β (20 ng/mL; Peprotech). To avoid allogenic immune responses, PBMCs from the same donor with T_{reg} cells were used for isolating $CD4^+$ T cells and $CD8^+$ T cells. $CD4^+$ and $CD8^+$ T cells were separated using Mojosort Human CD4 Nanobeads (BioLegend) and EasySep Human $CD8^+$ T cell Enrichment Kit (STEMCELL Technologies), respectively. T cells were stained with CTV. A375-PD-L1-OKT3-Fluc cells were treated mitomycin C for 20 min at 37°C and then co-cultured with CTV-stained T cells at a T:A375 cell ratio of 5:1. Next, the isolated immunosuppressive autogenic T_{reg} cells were stained with CFSE (Invitrogen) and added into the A375-T cell co-culture. After 5 days of incubation, the immunosuppressive activity of T_{reg} cells was measured from the proliferation of CTV-stained $CD4^+$ and $CD8^+$ T cells via quantification of CTV dilution. The culture medium was collected and analyzed with ELISA for IL-2 (BioLegend).

Cell conjugation assay

CFSE-stained human $CD3^+$ T cells were stimulated with Dynabeads Human T-Activator CD3/CD28 (Invitrogen) for 48 h, and surface LAG3 expression on T cells was verified by flow cytometry. $LAG3^+$ T cells were incubated with A375-Fluc-PD-L1 cells (BFP-positive) at a T to A375 ratio of 1:1 for 1 h at 37°C. The conjugation ratio was calculated as the portion of CFSE/BFP double-positive events.

Antibodies and flow cytometry

Mouse and human single cells were stained with fluorochrome-conjugated antibodies for 20 min at 4°C after blocking with anti-mouse CD16/32 (BioLegend) and human TruStain FcX (BioLegend) in FACS buffer (phosphate-buffered saline [PBS] containing 1% BSA and 0.1% sodium azide). For intracellular staining, cells were fixed and permeabilized using a Cytofix/Cytoperm Kit (BD Biosciences) or Foxp3/Transcription Factor Staining Buffer Set (Invitrogen). The following fluorochrome-conjugated anti-human antibodies were used: anti-CD3 (HIT3a), anti-CD4 (OKT4), anti-CD8 (SK1), anti-CD11c (3.9), anti-CD14 (63D3), anti-CD19 (HIB19), anti-CD25 (BC96), anti-CD45RO (UCHL1), anti-CD56 (5.1H11), anti-CD62L (DREG-56), anti-CD69 (FN50), anti-CD80 (2D10), anti-CD86 (IT2.2), anti-CD96 (6F9), anti-4-1BB (4B4-1), anti-Lag3 (11C3C65), anti-CD226 (11A8), anti-PD-1 (EH12.2H7), anti-Tim3 (F38-2E2), anti-TIGIT (MBSA43), anti-HLA-DR (BB7.2), anti-HLA-ABC (W6/32), anti-Foxp3 (236A-E7), and anti-mouse-TCRβ (H57-597).

Luminex multiplex cytokine assay

To measure multi-cytokine production, human monocyte-derived DCs were stimulated with plate-bound parental anti-PD-L1 (10 μg/mL) or soluble parental anti-PD-L1 (10 μg/mL) for 48 h. Supernatants were collected, and cytokines were detected using Luminex assay kit (R&D systems) according to the manufacturer's instructions (R&D Systems).

Human samples and study approval

Blood samples were obtained from healthy donors and CCA patients who received adjuvant gemcitabine plus cisplatin (GemCis) after curative resection under the clinical trial (ClinicalTrials.gov identifier NCT03079427) approved by Asan Medical Center Institutional Review Board (2021-0677).

Mouse studies

Murine experiments were approved and performed in accordance with the guidelines of the Institutional Animal Care and Use Committees of the Asan Medical Center (201904103) or GemPharmatech (GPTAP20200713-4 and GPTAP20201230-2).

Xenogeneic tumor model

A375-PD-L1 tumor cells were implanted in the right flank of immune-deficient NSG mice (JA Bio, Suwon, Korea). After tumors were established (mean volume of 150 mm^3), the mice were randomly assigned into five groups. One group received a single intravenous tail-vein injection of PBS, and four groups were administered 1G4 TCR-expressing human $CD8^+$ T cells (2×10^6 cells). At 1 day following T cell transfer, mice were treated intraperitoneally every 3 days 4 times with human IgG (10 mg/kg), anti-PD-L1 (10 mg/kg), anti-LAG3 (10 mg/kg), or a molar equivalent amount of ABL501 (14 mg/kg). Tumor growth and body weight were measured every 3 days.

Syngeneic tumor model

Syngeneic tumor studies were carried out in BALB/c mice expressing human LAG-3 and PD-1 (BALB/c-hPD1/hLAG3, T004622; GemPharmatech) and C57BL/6 mice expressing human LAG-3, PD-1, and PD-L1 (C57BL/6-hPD1/hPDL1/hLAG3, T006876; GemPharmatech). hPD1/hLAG3 humanized mice (seven mice/group) were implanted with 2×10^6 CT26-hPD-L1(Tg)-mPD-L1(KO) colon cancer cells (GemPharmatech) by subcutaneous injection on the right flank. When the average tumor size reached 87 mm^3, antibodies were administered via intraperitoneal injection of hIgG1 (7.5 mg/kg), hPD-L1 (7.5 mg/kg), or ABL501(1, 3 or 10 mg/kg) three times at 7-day intervals. hLAG-3/hPD-1/hPD-L1 humanized mice (five mice/group) were implanted with 2×10^6 MC38-hPD-L1(Tg)-mPD-L1(KO) colon cancer cells (GemPharmatech) by subcutaneous injection on the right flank. ABL501 (10 mg/kg) or human IgG1 isotype control (8.5 mg/kg) was subsequently administered by intraperitoneal injection four times every 3 days. Tumor growth was monitored over time via caliper measurements. Mice were euthanized when the tumor size reached 2,500 mm^3.

Cytobank analysis

viSNE, FlowSOM, and CITRUS analyses were performed using Cytobank software (Beckman Coulter). For viSNE analysis, equal number of cells (1,000 cells) from each flow cytometry standard (FCS) file were used, and resulting viSNE maps were fed into FlowSOM analysis.[75] For each cell subset, a new self-organizing map was generated using hierarchical consensus clustering on the tSNE axes. For CITRUS analysis, association models of significance analysis of microarrays and nearest shrunken centroid were selected as statistical methods. Abundance mode was selected to quantify and characterize individual clusters in samples. The minimal cluster size was 3%, and the cross-validation fold was 5.[45]

Good Laboratory Practices toxicity study in cynomolgus monkeys

The cynomolgus monkey study was conducted in accordance with guidelines of the Institutional Animal Care and Use Committee (IACUC) (SZ20200416-monkeys). Cynomolgus monkeys (five/sex/group) were administered a slow intravenous injection of ABL501 at 0, 20, 60, or 200 mg/kg twice weekly, eight times (days 1, 4, 8, 11, 15, 18, 22, and 25). Necropsy was performed on day 29 for the main groups (three/sex/group), followed by a recovery period for 56 days (two/sex/group). Safety and toxicity were assessed based on standard parameters. The study was conducted in accordance with the Safety and Quality Assurance guidelines in the Guideline for Experiments Document of WuXiAppTec.

Statistical analysis

Statistical analyses were performed using the appropriate statistical comparison, including the two-tailed paired or unpaired Student's t test, one-way ANOVA with Holm-Sidak multiple comparisons, or two-way ANOVA with Tukey's multiple comparisons. $p < 0.05$ were considered statistically significant ($^*p < 0.05$, $^{**}p < 0.01$, $^{***}p < 0.001$, and $^{****}p < 0.0001$).

SUPPLEMENTAL INFORMATION

Supplemental information can be found online at https://doi.org/10.1016/j.ymthe.2022.05.003.

ACKNOWLEDGMENTS

We thank the core facilities of Genetically Engineered Animal Core and flow cytometry at the Convergence Medicine Research Center (CREDIT), Asan Medical Center. This work was supported by an intramural grant of KIST, by the National Research Foundation of Korea grants (NRF-2021R1A2C1003551 to H.J., NRF-2020M3A9G7103935 to H.J., and NRF-2021R1A2C2006647 to Y.P.), and by a grant of the Korea Health Technology R&D Project through the Korea Health Industry Development Institute, funded by the Ministry of Health & Welfare of South Korea (HI20C0117 to J. Jung).

AUTHOR CONTRIBUTIONS

Conception and design, E.S., E.P., Jonghwa Won, H.J., J. Jung, and Y.P.; development of methodology, E.S., M.K., H.J., J. Jung, and Y.P.; acquisition of data, Ju-young Won, Y.J., E.C., U.J., J. Jeon, Y.K., H.A., D.C., S.C., Y.H., H.P., H.L., Y.-G.S., and K.P.; technical and material support, S.J.O., S.L., K.K., C.Y., and H.K.S.; analysis and interpretation of data, E.S., E.P., H.K., H.P., H.L., Jonghwa Won, H.J., J. Jung, and Y.P.; writing the manuscript, E.S., H.J., J. Jung, and Y.P.; study supervision, H.J., J. Jung, and Y.P.

DECLARATION OF INTERESTS

E.S., E.P., H.K., U.J., J. Jeon, Y.K., Y.H., H.P., H.L., Y.-G.S., K.P., Jonghwa Won, and J. Jung are employees of ABL Bio Inc. The other authors declare no competing interests.

REFERENCES

1. Dunn, G.P., Old, L.J., and Schreiber, R.D. (2004). The three Es of cancer immunoediting. Annu. Rev. Immunol. *22*, 329–360. https://doi.org/10.1146/annurev.immunol.22.012703.104803.
2. Callahan, M.K., Postow, M.A., and Wolchok, J.D. (2016). Targeting T cell Co-receptors for cancer therapy. Immunity *44*, 1069–1078. https://doi.org/10.1016/j.immuni.2016.04.023.
3. McLane, L.M., Abdel-Hakeem, M.S., and Wherry, E.J. (2019). CD8 T cell exhaustion during chronic viral infection and cancer. Annu. Rev. Immunol. *37*, 457–495. https://doi.org/10.1146/annurev-immunol-041015-055318.
4. Shen, R.L., Postow, M.A., Adamow, M., Arora, A., Hannum, M., Maher, C., Wong, P., Curran, M.A., Hollmann, T.J., Jia, L.W., et al. (2021). LAG-3 expression on peripheral blood cells identifies patients with poorer outcomes after immune checkpoint blockade. Sci. Transl. Med. *13*, eabf5107. https://doi.org/10.1126/scitranslmed.abf5107.
5. Topalian, S.L., Hodi, F.S., Brahmer, J.R., Gettinger, S.N., Smith, D.C., McDermott, D.F., Powderly, J.D., Sosman, J.A., Atkins, M.B., Leming, P.D., et al. (2019). Five-year survival and correlates among patients with advanced melanoma, renal cell carcinoma, or non-small cell lung cancer treated with nivolumab. Jama Oncol. *5*, 1411–1420. https://doi.org/10.1001/jamaoncol.2019.2187.
6. Garon, E.B., Rizvi, N.A., Hui, R.N., Leighl, N., Balmanoukian, A.S., Eder, J.P., Patnaik, A., Aggarwal, C., Gubens, M., Horn, L., et al. (2015). Pembrolizumab for the treatment of non-small-cell lung cancer. N. Engl. J. Med. *372*, 2018–2028. https://doi.org/10.1056/NEJMoa1501824.
7. Zou, W.P., Wolchok, J.D., and Chen, L.P. (2016). PD-L1 (B7-H1) and PD-1 pathway blockade for cancer therapy: mechanisms, response biomarkers, and combinations. Sci. Transl. Med. *8*, 328rv4. https://doi.org/10.1126/scitranslmed.aad7118.
8. Triebel, F., Jitsukawa, S., Baixeras, E., Romanroman, S., Genevee, C., Viegaspequignot, E., and Hercend, T. (1990). Lag-3, a novel lymphocyte-activation gene closely related to Cd4. J. Exp. Med. *171*, 1393–1405. https://doi.org/10.1084/jem.171.5.1393.
9. Triebel, F. (2003). LAG-3: a regulator of T-cell and DC responses and its use in therapeutic vaccination. Trends Immunol. *24*, 619–622. https://doi.org/10.1016/j.it.2003.10.001.
10. Maruhashi, T., Sugiura, D., Okazaki, I.M., and Okazaki, T. (2020). LAG-3: from molecular functions to clinical applications. J. Immunother. Cancer *8*, e001014. https://doi.org/10.1136/jitc-2020-001014.
11. Maruhashi, T., Okazaki, I.M., Sugiura, D., Takahashi, S., Maeda, T.K., Shimizu, K., and Okazaki, T. (2018). LAG-3 inhibits the activation of CD4(+) T cells that recognize stable pMHCII through its conformation-dependent recognition of pMHCII. Nat. Immunol. *19*, 1415–1426. https://doi.org/10.1038/s41590-018-0217-9.
12. Maruhashi, T., Sugiura, D., Okazaki, I.M., Shimizu, K., Maeda, T.K., Ikubo, J., Yoshikawa, H., Maenaka, K., Ishimaru, N., Kosako, H., et al. (2022). Binding of LAG-3 to stable peptide-MHC class II limits T cell function and suppresses autoimmunity and anti-cancer immunity. Immunity *55*, 912–924.e8. https://doi.org/10.1016/j.immuni.2022.03.013.
13. Xu, F., Liu, J., Liu, D., Liu, B.A., Wang, M., Hu, Z.Y., Du, X.M., Tang, L., and He, F.C. (2014). LSECtin expressed on melanoma cells promotes tumor progression by inhibiting antitumor T-cell responses. Cancer Res. *74*, 3418–3428. https://doi.org/10.1158/0008-5472.Can-13-2690.
14. Kouo, T., Huang, L.Q., Pucsek, A.B., Cao, M.W., Solt, S., Armstrong, T., and Jaffee, E. (2015). Galectin-3 shapes antitumor immune responses by suppressing CD8(+) T cells via LAG-3 and inhibiting expansion of plasmacytoid dendritic cells. Cancer Immunol. Res. *3*, 412–423. https://doi.org/10.1158/2326-6066.Cir-14-0150.
15. Mao, X., Ou, M., Karuppagounder, S., Kam, T.I., Yin, X., Xiong, Y., Ge, P., Umanah, G., Brahmachari, S., Shin, J., et al. (2017). Pathological alpha-synuclein transmission initiated by binding lymphocyte-activation gene 3. Science *353*, aah3374.
16. Wang, J., Sanmamed, M.F., Datar, I., Su, T.T., Ji, L., Sun, J.W., Chen, L., Chen, Y.S., Zhu, G.F., Yin, W.W., et al. (2019). Fibrinogen-like protein 1 is a major immune inhibitory ligand of LAG-3. Cell *176*, 334–347.e12. https://doi.org/10.1016/j.cell.2018.11.010.
17. Huang, C.T., Workman, C.J., Flies, D., Pan, X., Marson, A.L., Zhou, G., Hipkiss, E.L., Ravi, S., Kowalski, J., Levitsky, H.I., et al. (2004). Role of LAG-3 in regulatory T cells. Immunity *21*, 503–513. https://doi.org/10.1016/j.immuni.2004.08.010.
18. Zhang, Q.X., Chikina, M., Szymczak-Workman, A.L., Horne, W., Kolls, J.K., Vignali, K.M., Normolle, D., Bettini, M., Workman, C.J., and Vignali, D.A.A. (2017). LAG3 limits regulatory T cell proliferation and function in autoimmune diabetes. Sci. Immunol. *2*, eaah4569. https://doi.org/10.1126/sciimmunol.aah4569.
19. Matsuzaki, J., Gnjatic, S., Mhawech-Fauceglia, P., Beck, A., Miller, A., Tsuji, T., Eppolito, C., Qian, F., Lele, S., Shrikant, P., et al. (2010). Tumor-infiltrating NY-ESO-1-specific CD8(+) T cells are negatively regulated by LAG-3 and PD-1 in human ovarian cancer. Proc. Natl. Acad. Sci. U S A *107*, 7875–7880. https://doi.org/10.1073/pnas.1003345107.
20. Wang, Y.X., Dong, T.Y., Xuan, Q.J., Zhao, H., Qin, L., and Zhang, Q.Y. (2018). Lymphocyte-activation gene-3 expression and prognostic value in neoadjuvant-treated triple-negative breast cancer. J. Breast Cancer *21*, 124–133. https://doi.org/10.4048/jbc.2018.21.2.124.
21. Shapiro, M., Herishanu, Y., Katz, Ben-Zion, Dezorella, N., Sun, C., Kay, S., Polliack, A., Avivi, I., Wiestner, A., and Perry, C. (2017). Lymphocyte activation gene 3: a novel therapeutic target in chronic lymphocytic leukemia. Haematologica *102*, 874–882. https://doi.org/10.3324/haematol.2016.148965.
22. Yi, Q., Zhixin, F., Yuanxiang, G., Wei, X., Bushu, X., Jingjing, Z., Huoying, C., Xinke, Z., Musheng, Z., Yao, L., and Xing, Z. (2019). LAG-3 expression on tumor-infiltrating T cells in soft tissue sarcoma correlates with poor survival. Cancer Biol. Med. *16*, 331. https://doi.org/10.20892/j.issn.2095-3941.2018.0306.
23. Woo, S.R., Turnis, M.E., Goldberg, M.V., Bankoti, J., Selby, M., Nirschl, C.J., Bettini, M.L., Gravano, D.M., Vogel, P., Liu, C.L., et al. (2012). Immune inhibitory molecules LAG-3 and PD-1 synergistically regulate T-cell function to promote tumoral immune escape. Cancer Res. *72*, 917–927. https://doi.org/10.1158/0008-5472.CAN-11-1620.
24. Huang, R.Y., Eppolito, C., Lele, S., Shrikant, P., Matsuzaki, J., and Odunsi, K. (2015). LAG3 and PD1 co-inhibitory molecules collaborate to limit CD8+ T cell signaling and dampen antitumor immunity in a murine ovarian cancer model. Oncotarget *6*, 27359–27377. https://doi.org/10.18632/oncotarget.4751.
25. Waugh, K.A., Leach, S.M., Moore, B.L., Bruno, T.C., Buhrman, J.D., and Slansky, J.E. (2016). Molecular profile of tumor-specific CD8(+) T cell hypofunction in a transplantable murine cancer model. J. Immunol. *197*, 1477–1488. https://doi.org/10.4049/jimmunol.1600589.
26. Goding, S.R., Wilson, K.A., Xie, Y., Harris, K.M., Baxi, A., Akpinarli, A., Fulton, A., Tamada, K., Strome, S.E., and Antony, P.A. (2013). Restoring immune function of tumor-specific CD4(+) T cells during recurrence of melanoma. J. Immunol. *190*, 4899–4909. https://doi.org/10.4049/jimmunol.1300271.
27. Tawbi, H.A., Schadendorf, D., Lipson, E.J., Ascierto, P.A., Matamala, L., Castillo Gutierrez, E., Rutkowski, P., Gogas, H.J., Lao, C.D., De Menezes, J.J., et al. (2022). Relatlimab and nivolumab versus nivolumab in untreated advanced melanoma. N. Engl. J. Med. *386*, 24–34. https://doi.org/10.1056/NEJMoa2109970.
28. Wang, J., Asch, A.S., Hamad, N., Weickhardt, A., Tomaszewska-Kiecana, M., Dlugosz-Danecka, M., Pylypenko, H., Bahadur, B., Ulahannan, S., Koucheki, J., et al. (2020). A phase 1, open-label study of MGD013, a bispecific DART® molecule binding PD-1 and LAG-3 in patients with relapsed or refractory diffuse large B-cell lymphoma. Blood *136*, 21–22. https://doi.org/10.1182/blood-2020-139868.
29. Kraman, M., Faroudi, M., Allen, N.L., Kmiecik, K., Gliddon, D., Seal, C., Koers, A., Wydro, M.M., Batey, S., Winnewisser, J., et al. (2020). FS118, a bispecific antibody targeting LAG-3 and PD-L1, enhances T-cell activation resulting in potent antitumor activity. Clin. Cancer Res. *26*, 3333–3344. https://doi.org/10.1158/1078-0432.Ccr-19-3548.
30. Yap, T., Wong, D., Hu-Lieskovan, S., Papadopoulos, K., Morrow, M., Grabowska, U., Gliddon, D., Holz, J.B., and LoRusso, P. (2020). 395 A first-in-human study of FS118, a tetravalent bispecific antibody targeting LAG-3 and PD-L1, in patients with advanced cancer and resistance to PD-(L)1 therapy. J. Immunother. Cancer *8*, A240. https://doi.org/10.1136/jitc-2020-SITC2020.0395.

31. Jiang, H.P., Ni, H.Q., Zhang, P., Guo, X.L., Wu, M., Shen, H.R., Wang, J., Wu, W.W., Wu, Z.H., Ding, J.Z., et al. (2021). PD-L1/LAG-3 bispecific antibody enhances tumor-specific immunity. Oncoimmunology *10*, 1943180. https://doi.org/10.1080/2162402x.2021.1943180.

32. Angal, S., King, D.J., Bodmer, M.W., Turner, A., Lawson, A.D., Roberts, G., Pedley, B., and Adair, J.R. (1993). A single amino acid substitution abolishes the heterogeneity of chimeric mouse/human (IgG4) antibody. Mol. Immunol. *30*, 105–108. https://doi.org/10.1016/0161-5890(93)90432-b.

33. Zhang, Q., Chikina, M., Szymczak-Workman, A.L., Horne, W., Kolls, J.K., Vignali, K.M., Normolle, D., Bettini, M., Workman, C.J., and Vignali, D.A.A. (2017). LAG3 limits regulatory T cell proliferation and function in autoimmune diabetes. Sci. Immunol. *2*, eaah4569. https://doi.org/10.1126/sciimmunol.aah4569.

34. Godfrey, W.R., Ge, Y.G., Spoden, D.J., Levine, B.L., June, C.H., Blazar, B.R., and Porter, S.B. (2004). In vitro-expanded human CD4(+)CD25(+) T-regulatory cells can markedly inhibit allogeneic dendritic cell-stimulated MLR cultures. Blood *104*, 453–461. https://doi.org/10.1182/blood-2004-01-0151.

35. Levitsky, J., Miller, J., Leventhal, J., Huang, X., Flaa, C., Wang, E., Tambur, A., Burt, R.K., Gallon, L., and Mathew, J.M. (2009). The human "Treg MLR": immune monitoring for FOXP3+ T regulatory cell generation. Transplantation *88*, 1303–1311. https://doi.org/10.1097/TP.0b013e3181bbee98.

36. Booth, N.J., McQuaid, A.J., Sobande, T., Kissane, S., Agius, E., Jackson, S.E., Salmon, M., Falciani, F., Yong, K., Rustin, M.H., et al. (2010). Different proliferative potential and migratory characteristics of human CD4+ regulatory T cells that express either CD45RA or CD45RO. J. Immunol. *184*, 4317–4326. https://doi.org/10.4049/jimmunol.0903781.

37. Sylwester, A.W., Mitchell, B.L., Edgar, J.B., Taormina, C., Pelte, C., Ruchti, F., Sleath, P.R., Grabstein, K.H., Hosken, N.A., Kern, F., et al. (2005). Broadly targeted human cytomegalovirus-specific CD4+ and CD8+ T cells dominate the memory compartments of exposed subjects. J. Exp. Med. *202*, 673–685. https://doi.org/10.1084/jem.20050882.

38. Kuipers, H., Muskens, F., Willart, M., Hijdra, D., van Assema, F.B., Coyle, A.J., Hoogsteden, H.C., and Lambrecht, B.N. (2006). Contribution of the PD-1 ligands/PD-1 signaling pathway to dendritic cell-mediated CD4+ T cell activation. Eur. J. Immunol. *36*, 2472–2482. https://doi.org/10.1002/eji.200635978.

39. Park, S.J., Namkoong, H., Doh, J., Choi, J.C., Yang, B.G., Park, Y., and Chul Sung, Y. (2014). Negative role of inducible PD-1 on survival of activated dendritic cells. J. Leukoc. Biol. *95*, 621–629. https://doi.org/10.1189/jlb.0813443.

40. Versteven, M., Van den Bergh, J.M.J., Marcq, E., Smits, E.L.J., Van Tendeloo, V.F.I., Hobo, W., and Lion, E. (2018). Dendritic cells and programmed death-1 blockade: a joint venture to combat cancer. Front. Immunol. *9*, 394. https://doi.org/10.3389/fimmu.2018.00394.

41. Robbins, P.F., Li, Y.F., El-Gamil, M., Zhao, Y., Wargo, J.A., Zheng, Z., Xu, H., Morgan, R.A., Feldman, S.A., Johnson, L.A., et al. (2008). Single and dual amino acid substitutions in TCR CDRs can enhance antigen-specific T cell functions. J. Immunol. *180*, 6116–6131. https://doi.org/10.4049/jimmunol.180.9.6116.

42. Tian, Z., Liu, M., Zhang, Y., and Wang, X. (2021). Bispecific T cell engagers: an emerging therapy for management of hematologic malignancies. J. Hematol. Oncol. *14*, 75. https://doi.org/10.1186/s13045-021-01084-4.

43. Valle, J., Wasan, H., Palmer, D.H., Cunningham, D., Anthoney, A., Maraveyas, A., Madhusudan, S., Iveson, T., Hughes, S., Pereira, S.P., et al. (2010). Cisplatin plus gemcitabine versus gemcitabine for biliary tract cancer. N. Engl. J. Med. *362*, 1273–1281. https://doi.org/10.1056/NEJMoa0908721.

44. Park, J.O., Oh, D.Y., Hsu, C., Chen, J.S., Chen, L.T., Orlando, M., Kim, J.S., and Lim, H.Y. (2015). Gemcitabine plus cisplatin for advanced biliary tract cancer: a systematic Review. Cancer Res. Treat. *47*, 343–361. https://doi.org/10.4143/crt.2014.308.

45. Bruggner, R.V., Bodenmiller, B., Dill, D.L., Tibshirani, R.J., and Nolan, G.P. (2014). Automated identification of stratifying signatures in cellular subpopulations. Proc. Natl. Acad. Sci. U S A *111*, E2770–E2777. https://doi.org/10.1073/pnas.1408792111.

46. Ascierto, P.A., Melero, I., Bhatia, S., Bono, P., Sanborn, R.E., Lipson, E.J., Callahan, M.K., Gajewski, T., Gomez-Roca, C.A., Hodi, F.S., et al. (2017). Initial efficacy of anti-lymphocyte activation gene-3 (anti-LAG-3; BMS-986016) in combination with nivolumab (nivo) in pts with melanoma (MEL) previously treated with anti-PD-1/PD-L1 therapy. J. Clin. Oncol. *35*, 9520. https://doi.org/10.1200/JCO.2017.35.15_suppl.9520.

47. Sordo-Bahamonde, C., Lorenzo-Herrero, S., Gonzalez-Rodriguez, A.P., Payer, A.R., Gonzalez-Garcia, E., Lopez-Soto, A., and Gonzalez, S. (2021). LAG-3 blockade with relatlimab (BMS-986016) restores anti-leukemic responses in chronic lymphocytic leukemia. Cancers *13*, 2112. https://doi.org/10.3390/cancers13092112.

48. Heinhuis, K.M., Ros, W., Kok, M., Steeghs, N., Beijnen, J.H., and Schellens, J.H.M. (2019). Enhancing antitumor response by combining immune checkpoint inhibitors with chemotherapy in solid tumors. Ann. Oncol. *30*, 219–235. https://doi.org/10.1093/annonc/mdy551.

49. Trevejo, J.M., Marino, M.W., Philpott, N., Josien, R., Richards, E.C., Elkon, K.B., and Falck-Pedersen, E. (2001). TNF-alpha -dependent maturation of local dendritic cells is critical for activating the adaptive immune response to virus infection. Proc. Natl. Acad. Sci. U S A *98*, 12162–12167. https://doi.org/10.1073/pnas.211423598.

50. Raeber, M.E., Rosalia, R.A., Schmid, D., Karakus, U., and Boyman, O. (2020). Interleukin-2 signals converge in a lymphoid-dendritic cell pathway that promotes anticancer immunity. Sci. Transl. Med. *12*, eaba5464. https://doi.org/10.1126/scitranslmed.aba5464.

51. Frasca, L., Nasso, M., Spensieri, F., Fedele, G., Palazzo, R., Malavasi, F., and Ausiello, C.M. (2008). IFN-gamma arms human dendritic cells to perform multiple effector functions. J. Immunol. *180*, 1471–1481. https://doi.org/10.4049/jimmunol.180.3.1471.

52. Casati, C., Camisaschi, C., Rini, F., Arienti, F., Rivoltini, L., Triebel, F., Parmiani, G., and Castelli, C. (2006). Soluble human LAG-3 molecule amplifies the in vitro generation of type 1 tumor-specific immunity. Cancer Res. *66*, 4450–4460. https://doi.org/10.1158/0008-5472.CAN-05-2728.

53. Avice, M.N., Sarfati, M., Triebel, F., Delespesse, G., and Demeure, C.E. (1999). Lymphocyte activation gene-3, a MHC class II ligand expressed on activated T cells, stimulates TNF-alpha and IL-12 production by monocytes and dendritic cells. J. Immunol. *162*, 2748–2753.

54. Andreae, S., Piras, F., Burdin, N., and Triebel, F. (2002). Maturation and activation of dendritic cells induced by lymphocyte activation gene-3 (CD223). J. Immunol. *168*, 3874–3880. https://doi.org/10.4049/jimmunol.168.8.3874.

55. Andreae, S., Buisson, S., and Triebel, F. (2003). MHC class II signal transduction in human dendritic cells induced by a natural ligand, the LAG-3 protein (CD223). Blood *102*, 2130–2137. https://doi.org/10.1182/blood-2003-01-0273.

56. Graydon, C.G., Mohideen, S., and Fowke, K.R. (2021). LAG3's enigmatic mechanism of action. Front. Immunol. *11*, 615317. https://doi.org/10.3389/fimmu.2020.615317.

57. Li, N., Wang, Y., Forbes, K., Vignali, K.M., Heale, B.S., Saftig, P., Hartmann, D., Black, R.A., Rossi, J.J., Blobel, C.P., et al. (2007). Metalloproteases regulate T-cell proliferation and effector function via LAG-3. EMBO J. *26*, 494–504. https://doi.org/10.1038/sj.emboj.7601520.

58. Matsuo, K., Yoshie, O., Kitahata, K., Kamei, M., Hara, Y., and Nakayama, T. (2021). Recent progress in dendritic cell-based cancer immunotherapy. Cancers *13*, 2495. https://doi.org/10.3390/cancers13102495.

59. den Haan, J.M., Lehar, S.M., and Bevan, M.J. (2000). CD8(+) but not CD8(-) dendritic cells cross-prime cytotoxic T cells in vivo. J. Exp. Med. *192*, 1685–1696. https://doi.org/10.1084/jem.192.12.1685.

60. Pooley, J.L., Heath, W.R., and Shortman, K. (2001). Cutting edge: intravenous soluble antigen is presented to CD4 T cells by CD8- dendritic cells, but cross-presented to CD8 T cells by CD8+ dendritic cells. J. Immunol. *166*, 5327–5330. https://doi.org/10.4049/jimmunol.166.9.5327.

61. Mizumoto, Y., Hemmi, H., Katsuda, M., Miyazawa, M., Kitahata, Y., Miyamoto, A., Nakamori, M., Ojima, T., Matsuda, K., Nakamura, M., et al. (2020). Anticancer effects of chemokine-directed antigen delivery to a cross-presenting dendritic cell subset with immune checkpoint blockade. Br. J. Cancer *122*, 1185–1193. https://doi.org/10.1038/s41416-020-0757-2.

62. Alexandre, Y.O., Ghilas, S., Sanchez, C., Le Bon, A., Crozat, K., and Dalod, M. (2016). XCR1+ dendritic cells promote memory CD8+ T cell recall upon secondary infections with Listeria monocytogenes or certain viruses. J. Exp. Med. *213*, 75–92. https://doi.org/10.1084/jem.20142350.

63. Matsuo, K., Kitahata, K., Kawabata, F., Kamei, M., Hara, Y., Takamura, S., Oiso, N., Kawada, A., Yoshie, O., and Nakayama, T. (2018). A highly active form of

XCL1/lymphotactin functions as an effective adjuvant to recruit cross-presenting dendritic cells for induction of effector and memory CD8(+) T cells. Front. Immunol. *9*, 2775. https://doi.org/10.3389/fimmu.2018.02775.

64. Jiang, H., Ni, H., Zhang, P., Guo, X., Wu, M., Shen, H., Wang, J., Wu, W., Wu, Z., Ding, J., et al. (2021). PD-L1/LAG-3 bispecific antibody enhances tumor-specific immunity. Oncoimmunology *10*, 1943180. https://doi.org/10.1080/2162402X.2021.1943180.

65. Moon, E.K., Ranganathan, R., Eruslanov, E., Kim, S., Newick, K., O'Brien, S., Lo, A., Liu, X., Zhao, Y., and Albelda, S.M. (2016). Blockade of programmed death 1 augments the ability of human T cells engineered to target NY-ESO-1 to control tumor growth after adoptive transfer. Clin. Cancer Res. *22*, 436–447. https://doi.org/10.1158/1078-0432.CCR-15-1070.

66. Dolina, J.S., Van Braeckel-Budimir, N., Thomas, G.D., and Salek-Ardakani, S. (2021). CD8(+) T cell exhaustion in cancer. Front. Immunol. *12*, 715234. https://doi.org/10.3389/fimmu.2021.715234.

67. Ghoneim, H.E., Zamora, A.E., Thomas, P.G., and Youngblood, B.A. (2016). Cell-intrinsic barriers of T cell-based immunotherapy. Trends Mol. Med. *22*, 1000–1011. https://doi.org/10.1016/j.molmed.2016.10.002.

68. Borst, J., Ahrends, T., Babala, N., Melief, C.J.M., and Kastenmuller, W. (2018). CD4(+) T cell help in cancer immunology and immunotherapy. Nat. Rev. Immunol. *18*, 635–647. https://doi.org/10.1038/s41577-018-0044-0.

69. Oh, D.Y., Kwek, S.S., Raju, S.S., Li, T., McCarthy, E., Chow, E., Aran, D., Ilano, A., Pai, C.C.S., Rancan, C., et al. (2020). Intratumoral CD4(+) T cells mediate anti-tumor cytotoxicity in human bladder cancer. Cell *181*, 1612–1625.e13. https://doi.org/10.1016/j.cell.2020.05.017.

70. Kagamu, H., Kitano, S., Yamaguchi, O., Yoshimura, K., Horimoto, K., Kitazawa, M., Fukui, K., Shiono, A., Mouri, A., Nishihara, F., et al. (2020). CD4(+) T-cell immunity in the peripheral blood correlates with response to anti-PD-1 therapy. Cancer Immunol. Res. *8*, 334–344. https://doi.org/10.1158/2326-6066.CIR-19-0574.

71. Takeuchi, Y., Tanemura, A., Tada, Y., Katayama, I., Kumanogoh, A., and Nishikawa, H. (2018). Clinical response to PD-1 blockade correlates with a sub-fraction of peripheral central memory CD4+ T cells in patients with malignant melanoma. Int. Immunol. *30*, 13–22. https://doi.org/10.1093/intimm/dxx073.

72. Sun, J.Y., Zhang, D., Wu, S., Xu, M., Zhou, X., Lu, X.J., and Ji, J. (2020). Resistance to PD-1/PD-L1 blockade cancer immunotherapy: mechanisms, predictive factors, and future perspectives. Biomark. Res. *8*, 35. https://doi.org/10.1186/s40364-020-00212-5.

73. Jin, H.S., Ko, M., Choi, D.S., Kim, J.H., Lee, D.H., Kang, S.H., Kim, I., Lee, H.J., Choi, E.K., Kim, K.P., et al. (2020). CD226(hi)CD8(+) T cells are a prerequisite for anti-TIGIT immunotherapy. Cancer Immunol. Res. *8*, 912–925. https://doi.org/10.1158/2326-6066.CIR-19-0877.

74. Lee, D.H., Kang, S.H., Choi, D.S., Ko, M., Choi, E., Ahn, H., Min, H., Oh, S.J., Lee, M.S., Park, Y., and Jin, H.S. (2021). Genome wide CRISPR screening reveals a role for sialylation in the tumorigenesis and chemoresistance of acute myeloid leukemia cells. Cancer Lett. *510*, 37–47. https://doi.org/10.1016/j.canlet.2021.04.006.

75. Quintelier, K., Couckuyt, A., Emmaneel, A., Aerts, J., Saeys, Y., and Van Gassen, S. (2021). Analyzing high-dimensional cytometry data using FlowSOM. Nat. Protoc. *16*, 3775–3801. https://doi.org/10.1038/s41596-021-00550-0.

YMTHE, Volume *30*

Supplemental Information

LAG-3xPD-L1 bispecific antibody potentiates antitumor responses of T cells through dendritic cell activation

Eunsil Sung, Minkyung Ko, Ju-young Won, Yunju Jo, Eunyoung Park, Hyunjoo Kim, Eunji Choi, Ui-jung Jung, Jaehyoung Jeon, Youngkwang Kim, Hyejin Ahn, Da-som Choi, Seunghyun Choi, Youngeun Hong, Hyeyoung Park, Hanbyul Lee, Yong-Gyu Son, Kyeongsu Park, Jonghwa Won, Soo Jin Oh, Seonmin Lee, Kyu-pyo Kim, Changhoon Yoo, Hyun Kyu Song, Hyung-seung Jin, Jaeho Jung, and Yoon Park

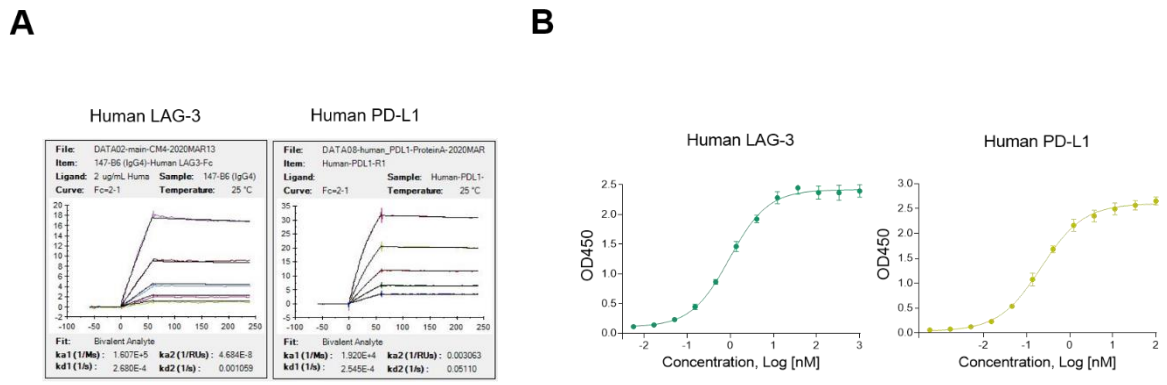

Figure S1. Measurement of the LAG-3 or PD-L1 binding affinity of ABL501

(A) SPR analysis of ABL501 binding against human recombinant LAG-3 (left) and PD-L1 (right). The binding affinity (K_D) of ABL501 was 2.0 nM to human LAG-3 and 16 nM to human PD-L1. (B) ELISA of ABL501 binding to human recombinant LAG-3 (left, EC_{50}=0.958 nM) and PD-L1 (right, EC_{50}=0.532 nM). Data were pooled from three independent experiments.

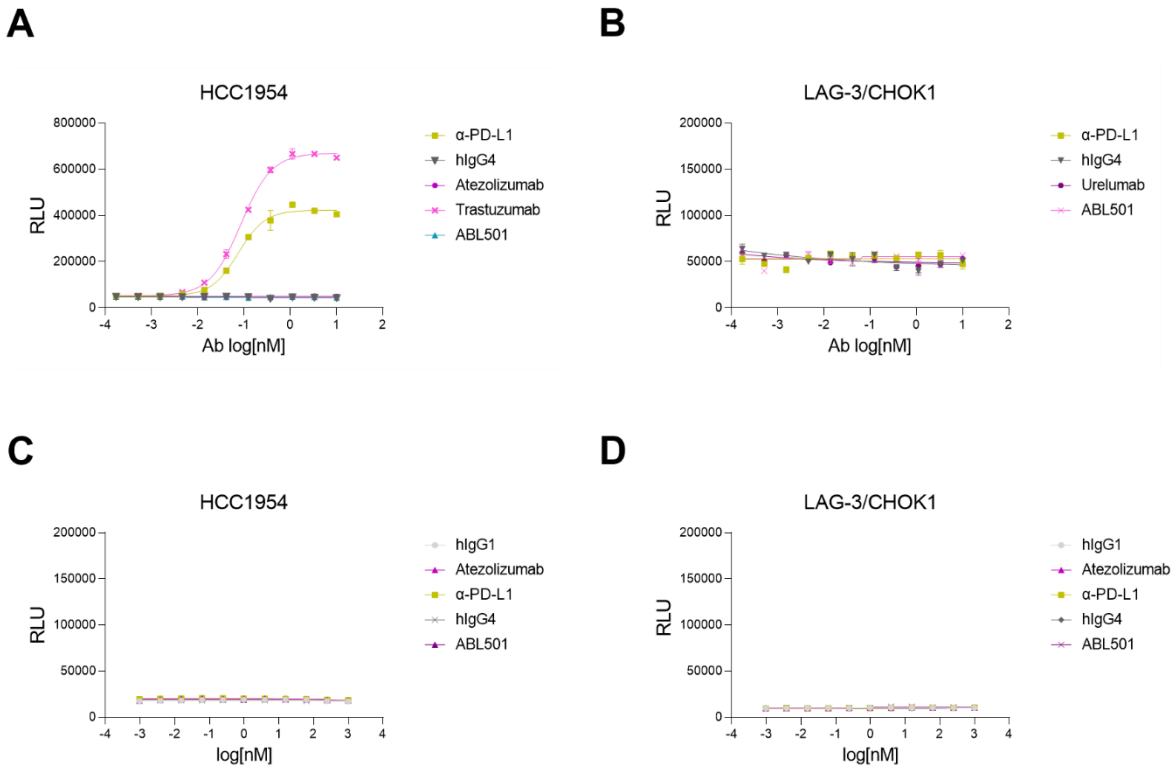

Figure S2. Measurement of Fc-mediated effector functions of ABL501

(A-B) ADCC activity of ABL501 was evaluated by co-incubation of NFAT-reporter Jurkat cells expressing hFcγRIIIa-V158 variant with tumor cells expressing PD-L1 or LAG-3. Measurement of ADCC activity of the indicated antibodies against (A) HCC1954 cells expressing PD-L1 or (B) CHOK1 cells expressing LAG-3. (C-D) CDC activity of ABL501 was evaluated in tumor cells expressing PD-L1 or LAG-3 via co-incubation with human complement serum. Measurement of CDC activity of the indicated antibodies in (C) HCC1954 cells expressing PD-L1 or (D) CHOK1 cells expressing LAG-3. Data were pooled from three independent experiments.

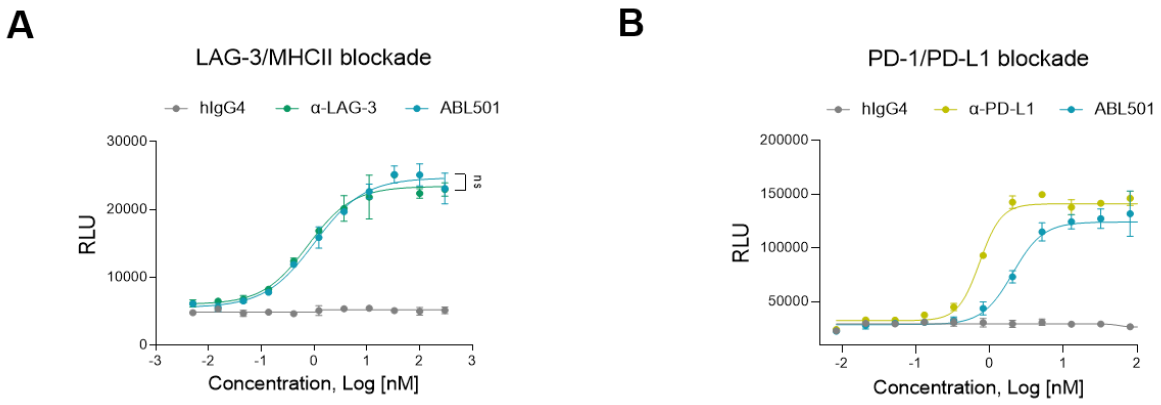

Figure S3. Inhibition of PD-1/PD-L1 or LAG-3/MHC-II signaling by ABL501

(A-B) The effect of ABL501 on LAG-3/MHC-II or PD-1/PD-L1 signaling was assessed by co-incubation of NF-κB-Luc2/LAG-3 or PD-1 reporter Jurkat cells with target cells expressing MHC-II or PD-L1 (Bioassay). (A) Blocking activity of ABL501 or anti-LAG-3 against LAG-3/MHC-II was measured by luciferase activity assay in NF-κB-Luc2/LAG-3 reporter Jurkat cells. (ABL501: EC_{50}=0.84 nM, anti-LAG-3: EC_{50}=0.60 nM). (B) Blocking activity of ABL501 or anti-PD-L1 against PD-1/PD-L1 was measured by luciferase activity assay in NF-κB-Luc2/PD-1 reporter Jurkat cells. (ABL501: EC_{50}=2.8 nM, anti-PD-L1: EC_{50}=0.72 nM). Data were pooled from three independent experiments.

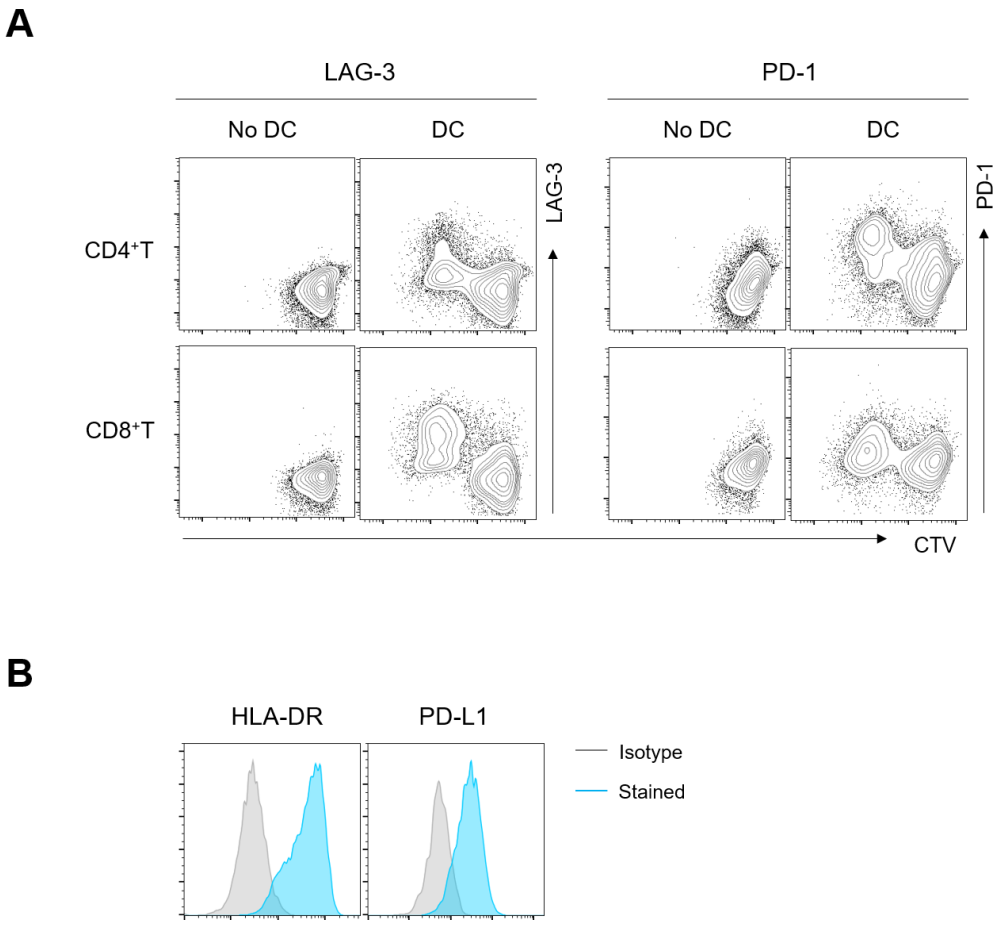

Figure S4. Upregulation of LAG-3 and PD-1 expressions by T cells upon stimulation with allogeneic mo-DCs

$CD4^+$T or $CD8^+$Tcells isolated from PBMCs were co-cultured with allogeneic mo-DCs in the presence of anti-human IgG antibody at a final concentration of 33.4 nM for 5 days. (A) FACS analysis showing LAG-3 and PD-1 expressions in CTV_{low} $CD4^+$ or $CD8^+$T cells. (B) FACS histograms showing the expression of HLA-DR and PD-L1 in mo-DCs.

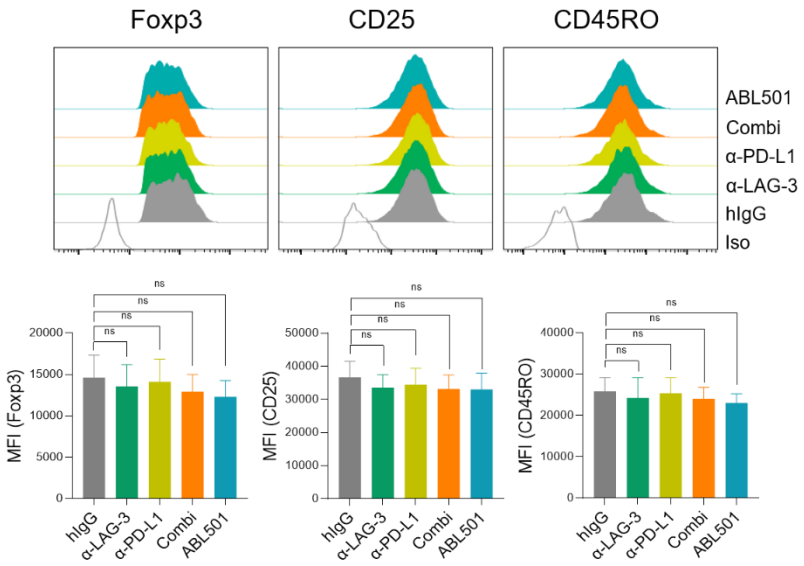

Figure S5. Effect of ABL501 on phenotypic characteristics of T_{reg} cells

Isolated and ex vivo expanded Treg cells were co-cultured with A375-OKT3 cells in the presence of the indicated antibodies at a final concentration of 66.8 nM. Representative FACS histograms (above) and summary graphs (below) showing the expression of Foxp3, CD25 and CD45RO in T_{reg} cells. Data were compiled from three independent experiments with two replicates. Statistical significance was determined by one-way ANOVA with Holm–Sidak multiple comparisons. ns: not significant.

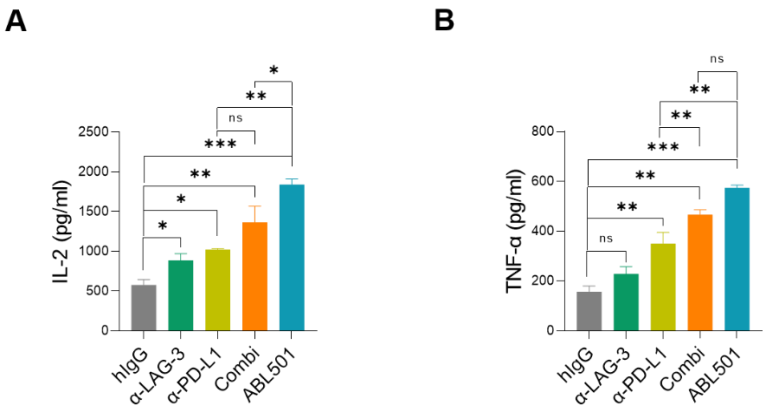

Figure S6. ABL501 increases IL-2 and TNF-α secretion by T cells upon stimulation with CMV lysate

(A-B) CTV-stained PBMCs were stimulated with CMV lysate in the presence of the indicated antibodies at a final concentration of 66.8 nM for 5 days. ELISA of IL-2 (A) or TNF-α (B) secretion by CMV-responsive T cells with the indicated antibodies. Data were pooled from three independent experiments with two replicates. Statistical significance was determined by one-way ANOVA with Holm–Sidak multiple comparisons. *p<0.05, **p<0.01, ***p<0.001, ns: not significant.

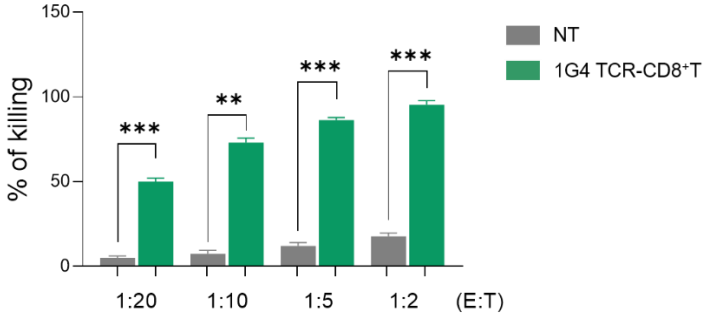

Figure S7. NY-ESO-1-specific killing of A375 cells by 1G4 TCR-CD8$^+$T cells

NT, or 1G4 TCR-CD8$^+$T cells were co-cultured with A375 cells expressing luciferase at variable E:T ratios for 2 days. A375 cell killing was measured by luciferase activity. Bar graph showing percentages of A375 cell killing by NT or 1G4 TCR-CD8$^+$T cells. Data were pooled from three independent experiments with three replicates. Statistical significance was determined by paired *t*-tests with two-tailed analysis. $^{**}p<0.01$ and $^{***}p<0.001$

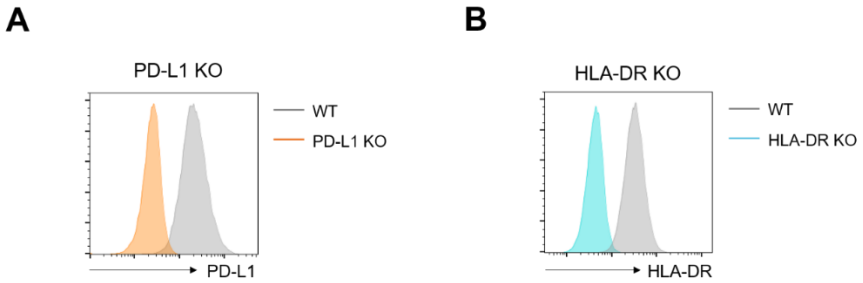

Figure S8. Establishment of HLA-DR KO or PD-L1 KO A375 cells

(A) Flow cytometric analysis of the surface expression of PD-L1 in A375-WT (parental) and A375 PD-L1 KO cells after immunostaining with a fluorochrome-conjugated anti-PD-L1 antibody. (B) Flow cytometric analysis of the surface expression of HLA-DR in A375-WT (parental) and A375 HLA-DR KO cells after immunostaining with a fluorochrome-conjugated anti-HLA-DR antibody.

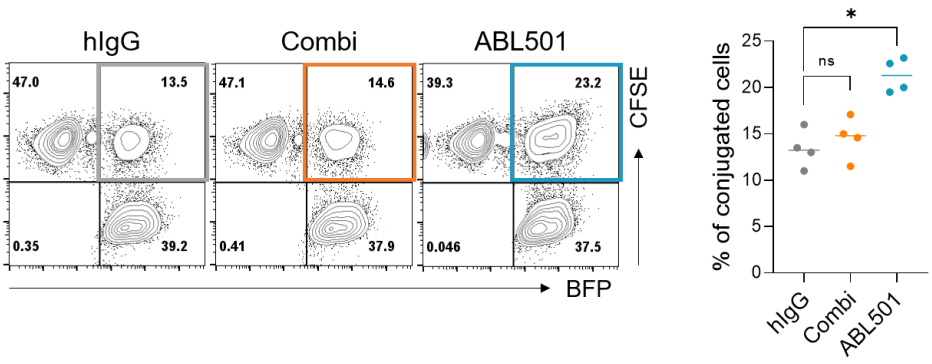

Figure S9. Effect of ABL501 on CD4^{+}T cell conjugation with tumor cells

CFSE-labeled CD4^{+}T cells expressing LAG-3 by pre-activation with anti-CD3/CD28 antibodies were incubated with A375-OKT3-PD-L1 cells for 30 min in the presence of the indicated antibodies and followed by FACS analysis. Representative FACS plots (left panel) and a summary plot (right panel) showing the percentages of BFP and CFSE double-positive populations in the presence of the indicated antibodies. Data were compiled from two independent experiments with two replicates. Statistical significance was determined by one-way ANOVA with Holm–Sidak multiple comparisons. *p<0.05, ns: not significant.

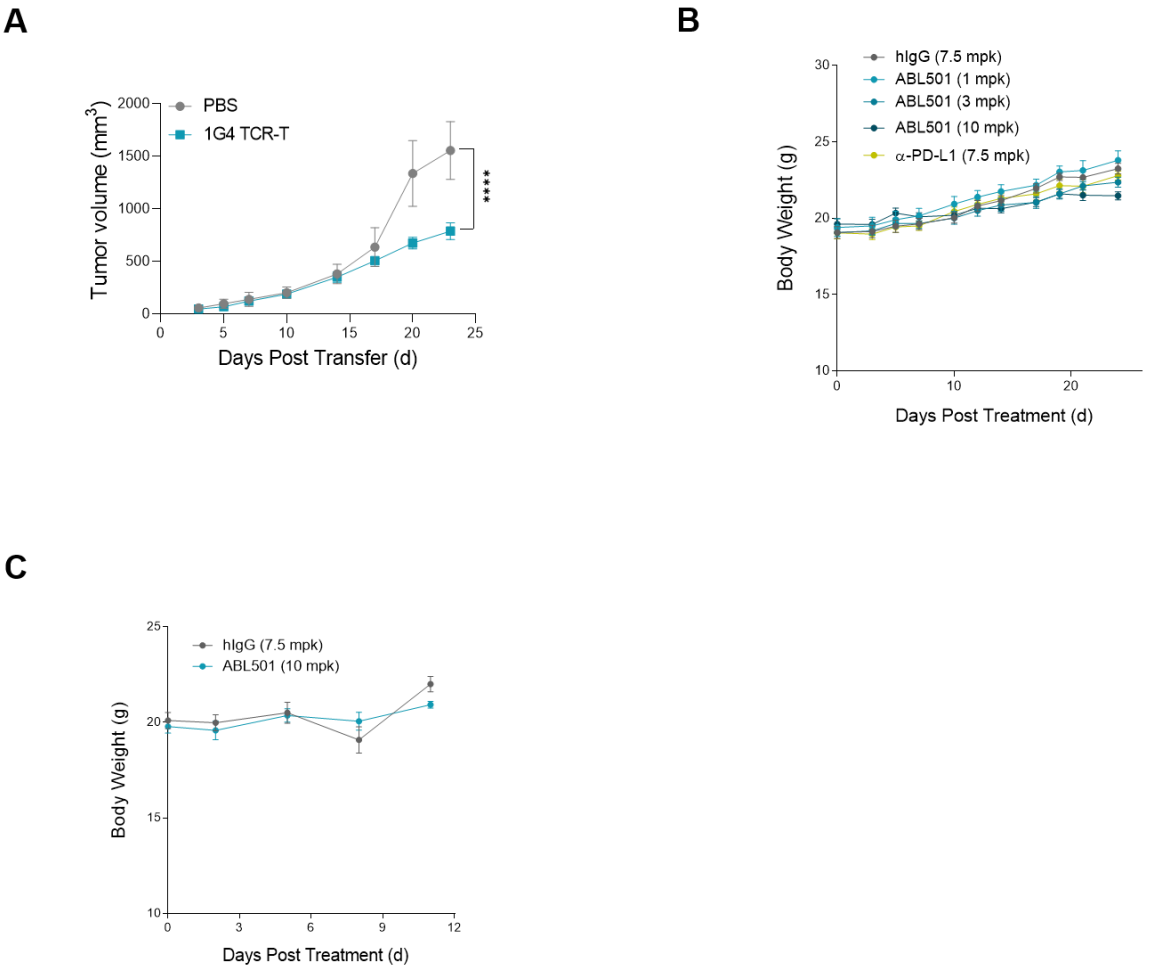

Figure S10. ABL501 inhibits tumor growth in humanized mouse models

(A) Tumor volume of NSG mice bearing A375-PD-L1 following adoptive transfer with $CD8^{+}$T cells expressing an NY-ESO-specific TCR. (B) Graphs of body weight change in human LAG-3/PD-1 knock-in BALB/c mice. (C) Graphs of body weight change in human LAG-3/PD-1/PD-L1 knock-in C57BL/6 mice. Significant differences between groups were determined by Two-way ANOVA Tukey's multiple comparison test. ****p <0.001.

A

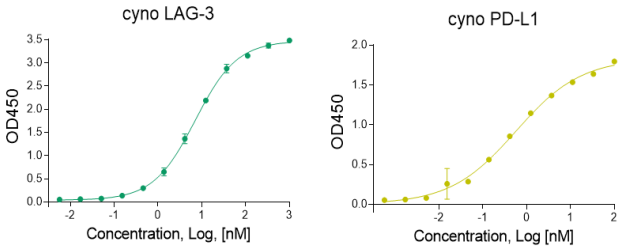
cyno LAG-3
OD450
Concentration, Log, [nM]
cyno PD-L1
OD450
Concentration, Log [nM]

B

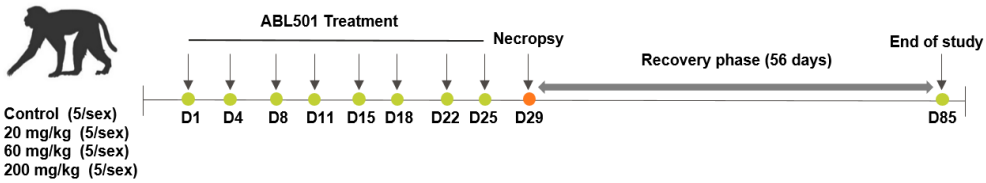
ABL501 Treatment
Necropsy
Recovery phase (56 days)
End of study
D1 D4 D8 D11 D15 D18 D22 D25 D29
D85
Control (5/sex)
20 mg/kg (5/sex)
60 mg/kg (5/sex)
200 mg/kg (5/sex)

C

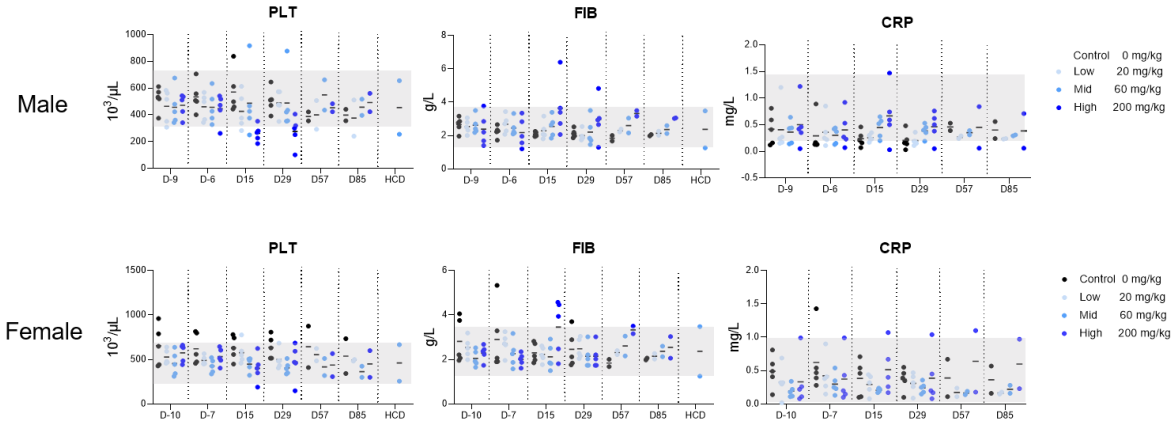
Male
PLT
FIB
CRP
Female
Control 0 mg/kg
Low 20 mg/kg
Mid 60 mg/kg
High 200 mg/kg

D

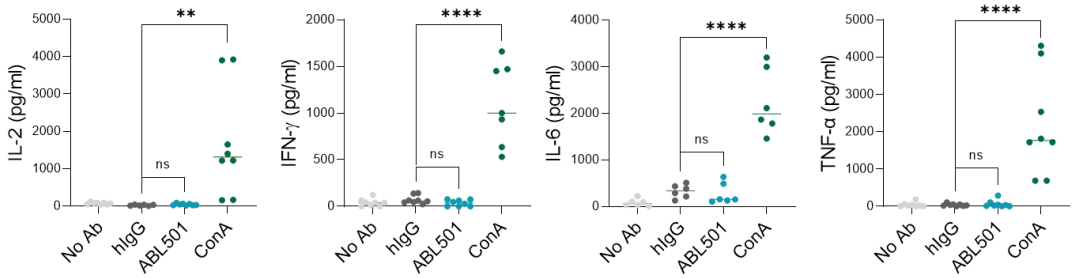
IL-2 (pg/ml)
IFN-γ (pg/ml)
IL-6 (pg/ml)
TNF-α (pg/ml)
No Ab
hIgG
ABL501
ConA
ns

Figure S11. ABL501 exhibits a safe toxicity profile in non-human primates

(A) ELISA of ABL501 binding to cynomolgus recombinant LAG-3 (left, EC50=7.05 nM) and PD-L1 (right, EC50=0.532 nM). Data were pooled from three independent experiments. (B) A schematic overview of the safety study in cynomolgus monkeys. Cynomolgus monkeys were administered twice weekly doses of ABL501 at 20, 60, and 200 mg/kg for up to 8 times. Necropsies were performed on day 29 after the first dose. (C) Platelet (PLT) number, fibrinogen (FIB), and C-reactive protein (CRP) were measured over time. Gray areas denote the historical normal range. (D) ELISA of IL-2, IFN-γ, IL-6, and TNF-α production by human PBMC cultured for 48 h in the presence or absence of hIgG1 (1 μg/well) or ABL501 (1.4 μg/well). Concanavalin A (Con A) at 5 μg/mL was used as a positive control. Each dot represents an individual human sample. Statistical significance was determined by one-way ANOVA with Holm–Sidak multiple comparisons in (D). $^{**}p<0.01$ and $^{****}p<0.0001$, ns: not significant.

Patient characteristics

Variable	Non-relapsed (N=9)	Relapsed (N=11)
Age (yr)	64 (52-75)	62.6 (53-74)
Sex		
Male	8	8
Female	1	3

Figure S12. Cholangiocarcinoma (CCA) patient characteristics

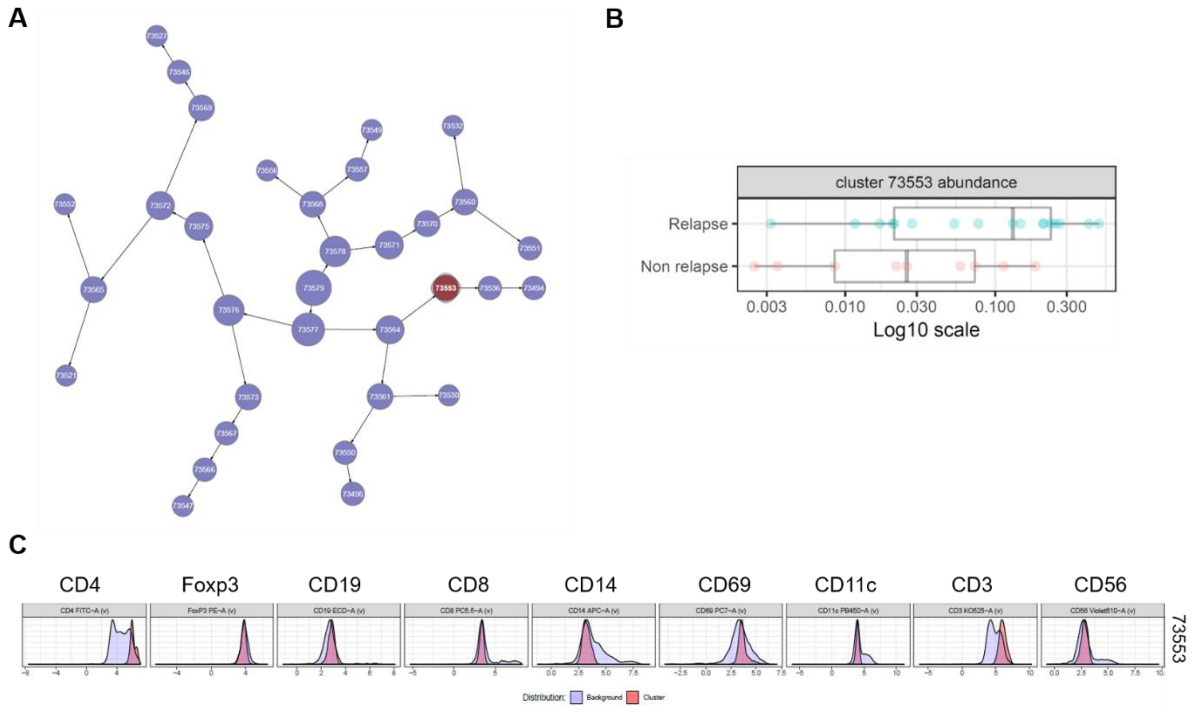

Figure S13. CITRUS analysis of peripheral blood immune cells in CCA patients

(A) CITRUS plot showing clusters from CCA patients in two groups (Relapse vs Non-relapse). The red dot represents a cluster that showed a different abundance with a statistical significance between groups. (B) Bar graphs showing the relevance of abundance for the selected cluster (red dot) between groups. (C) Histogram plots showing each marker expression by the selected cluster (red) over background (light blue).

Supplementary Methods

Expression and purification of recombinant antibodies

ExpiCHO-S cells were cultured in ExpiCHO expression medium (A2910001; Thermo Fisher) in a humidified shaking incubator at 37℃ with 8% CO_2. Transfection of ExpiCHO cells was performed using an ExpiCHO Expression System Kit (A29133; Thermo Fisher) according to the manufacture's protocol. Briefly, ExpiFectamine CHO transfection reagent and plasmid DNA were separately diluted in OptiPRO SFM (12309019; Thermo Fisher) and incubated at room temperature for 5 min. ExpiFectamine CHO-DNA-OptiPRO mixture was added to the cells (6×10^6 cells). At 18-22 h post-transfection, ExpiFectamine CHO Transfection Enhancer and ExpiFectamine CHO Transfection Feed were added, and the cells were further incubated for 7 days. Each antibody was purified from the cell culture supernatant by recombinant Protein A affinity chromatography (HiTram MabSelect SuRe, 28-4082-55; GE Healthcare). Equilibration was carried out using buffer (50 mM Tris-HCl, pH 7.4), and the sample was loaded onto the equilibrated column. The recombinant antibody was eluted with elution buffer (50 mM citrate, pH 3.4) and then neutralized to pH 6.5 using 1 M Tris-HCl (pH 9.0). Purified antibodies were concentrated by ultrafiltration using an Amicon Ultra 15 30K device (MilliporeSigma), and endotoxin levels of all antibodies were measured under 1.0 EU (endotoxin unit)/mg by Endosafe nexgen-PTS (Charles River Laboratories).

Enzyme-linked Immunosorbent assay (ELISA)

The binding properties of ABL501 against LAG-3 or PD-L1 proteins (human or monkey) was analyzed by ELISA. ELISA for PD-L1 proteins was performed at 37℃, whereas the LAG-3 binding assay was carried out at 25℃. Each well of the 96-well plate was coated with 0.5 μg/mL of human PD-L1 (10084-H08H; Sino Biological), monkey PD-L1 (90251-C08H; Sino

Biological), human LAG-3 (16498-H08H; Sino Biological), or 2 μg/mL of monkey LAG-3 (9992-L3; R&D Systems) overnight at 4℃. Diluted antibodies in blocking solution was added to the plate, which was then incubated for 1 h. After washing, diluted anti-human IgG Fc HRP conjugated antibody (31413; Pierce) in blocking solution was added, and the plate was incubated at for 1 h. The reaction was stopped by the addition of 50 μL/well of 0.5 N H_2SO_4 following 100 μL/well of tetramethylbenzidine (T0440; MilliporeSigma) treatment. The absorbance was measured with an ELISA plate reader at 450 nm (calibration: 650 nm) within 5 min, and the data were analyzed using the four-parameter logistics equation from the SoftMax Pro 5.4 software (Molecular Device).

Surface plasmon resonance (SPR)

(1) PD-L1 binding assay

ABL501 was diluted with 1xHBS-EP (BR100669; Cytiva) containing 500 mM NaCl and 2% (w/v) BSA, and then captured on the surface of the Protein A chip (29-1275-56; Cytiva) as approximately 370 RU. Two-fold serial diluted human PD-L1 (9049-B7; R&D systems) or monkey (cynomolgus) PD-L1 (10145-B7; R&D systems) with 1xHBS-EP from 500 to 31.25 nM were injected over the ABL501-captured surface for 60 s at 30 μL/min, and then 1xHBS-EP buffer was flown on the ABL501-PD-L1 complex for 180 s to monitor the complex dissociation. After that, 10 mM Glycine-HCl pH 1.5 (BR100354; Cytiva) was injected on the chip surface for 30 s at 30 μL/min. Kinetic analysis was performed using the bivalent analyte model in the BiaEvaluation software (version.01; Cytiva). All assay temperature was set as 25 ℃.

(2) LAG-3 binding assay

Human LAG-3 (2319-L3; R&D systems) or monkey (cynomolgus) LAG-3 (LA3-C5252; Acro Biosystems) were immobilized on the surface of the CM4 chip (BR100534; Cytiva) as approximately 100 RU with the amine coupling method. Two-fold serial diluted ABL501 with 50 mM sodium phosphate containing 150 mM NaCl pH 7.0 from 12.5 to 0.781 nM was injected on the LAG-3 immobilized chip surface for 60 s, and the LAG-3-ABL 501 complex was dissociated for 180 s using 50 mM sodium phosphate with 150 mM NaCl (pH 7.0) to monitor the complex dissociation. Kinetic analysis was performed using the bivalent analyte model in the BiaEvaluation software (version.01; Cytiva). All assay temperature was set as 25 ℃.

Flow cytometry-based antibody binding assay

The cell surface binding of ABL501 to tumor cells or target-positive engineered cell lines was measured by flow cytometry. Cells were incubated with varying concentrations of each antibody followed by a secondary antibody (FITC-conjugated anti-human Fc, F9512; Sigma). hIgG antibody was used as a negative control. EC_{50} value was determined using the GraphPad Prism software (version 8.3.0; GraphPad).

Antibody-dependent cellular cytotoxicity (ADCC) and complement-dependent cytotoxicity (CDC) assays

ADCC was determined using an ADCC reporter bioassay kit (Promega) following the protocol provided by the supplier. For CDC assay, target cells (1×10^4/100 μL per well) were plated in a 96-well plate. Serially diluted antibodies were added, and 25 μL of 2-fold diluted human complement serum (Quidel) was added to the well, followed by incubation for 5 h at 37 ℃ in 5% CO_2 incubator. Next, 75 μL of CytoTox-Glo reagent (Promega) was added to each well, and luminescence was measured using a plate reader (PHERAstar).

Luciferase reporter assays

ABL501-mediated regulation of PD-1 inhibitory signaling was assessed using human PD-L1-expressing CHO-K1 cells and Jurkat effector cells (JA011, Promega). Jurkat effector cells express human PD-1 and a luciferase reporter driven by NF-κB response elements. The ability of ABL501 to block LAG-3 inhibitory signaling was tested in LAG-3/MHCII Blockade Bioassay (JA2111, Promega). The bioassay consists of two cell lines: Jurkat effector cells expressing human LAG-3 and a luciferase reporter driven by T-cell activation pathway-dependent response elements; human MHC-II^+ antigen presenting cells (APC) expressing TCR activating surface molecule. Assays were performed according to the manufacturer's instructions (Promega). Data were analyzed as RLU, and the EC_{50} value was obtained using the GraphPad Prism software (version 8.3.0; GraphPad).